

We would like to thank the reviewers for dedicating their time to provide constructive feedback on our manuscript, which has now improved from the original submission. We want to point out that line numbers listed below correspond to those in the revision and not the track changes version attached to this review.

Reviewer #1

This is a well-written and interesting paper documenting the transport of wildfire smoke from the Pacific Northwest into Colorado. The paper is organized around specific events that resulted in degraded air quality and visibility through the Front Range of Colorado. Supporting evidence was provided through a variety of measurement platforms, including remote sensing and ground based measurements, as well as meteorological data and back trajectory analyses to describe the flow patterns during the events. The authors have combined these data into an interesting story that informs as to the transport of smoke across the United States with impacts on local air quality. An important result is the transport of mineral aerosols with the smoke plume. I recommend the paper be published after addressing the comments below.

We thank the reviewer for his/her positive support and constructive review.

Line 133: “g μm^{-3} ” typo.

Typo fixed.

Line 185: The authors repeatedly refer to “hazy” conditions along the Front Range (specifically Denver) and support the degraded air quality using PM data measured by the Colorado Department of Public Health and Environment. In checking the available data it appears that extinction data are also available from transmissometer measurements at the DESCi site. It would improve the paper to include these data so that the “hazy” can be quantified (line 185). In fact, the extinction values agree fairly closely with the TOPAZ lidar data in Figure 17 (given the wavelength differences).

Thank you for pointing this out. We now include the DESCi site in Figure 1, include the DESCi beta extinction data in Figure 3, describe the site and extinction data in the methods (section 2.2), discuss the extinction data when indicating a time period is hazy (section 3.1), and compare it to TOPAZ (first part of section 3.4).

Line 205: Please provide wavelength.

We now provide the wavelength (550 nm) in the methods when MODIS is first introduced (line 87).

Line 232, Section 3.3: This section is somewhat hard to follow because the figures are broken up so it requires flipping back and forth. I suggest organizing the figures so that, for example: the first event would include figure 7a-d, 8a, 9. It would reduce the number of figures and help to focus the discussion.

We have revised so that each event corresponds to one figure as suggested by the reviewer. Now, Figures 7, 8, and 9 contain the RAP, HYSPLIT, and profiler data from Events 1, 2, and 3, respectively. We also made sure this change was reflected throughout the text.

Line 244,245: Do the authors mean “northwesterly” here?

Yes, this was fixed.

Line 308: Figures 14-16 are similar enough it might be possible to just show one example.

We agree that the figures are strikingly similar. As a result, we have stated that the observations of smoke and dust from CALIPSO was consistent for all event days in the text and added the other two event CALIPSO figures to a Supporting Information file.

Line 333: A quick look at the IMPROVE data at the ROMO site in Rocky Mountain National Park also showed increased soil concentrations on 8/22, further corroborating the regional impact.

Thank you for highlighting this. We also looked at fine mass, sulfur, and potassium concentrations, and those were also elevated on or near event days when IMPROVE samples were obtained (16, 22, 28 Aug). We evaluated the concentrations of these and soil on event versus non-event days in August, and noticed the concentrations for all were higher on the event days. We now discuss this in the text on lines 364-366 and added a figure showing the increased concentrations on event days as compared to non-event days in the Supporting Information.

Line 348: Consider replacing “small” with “low”. My first interpretation was with respect to particle size within the mode.

Done.

Line 367: While the hazy days corresponded to relatively high PM relative to non-hazy days, I am not sure this supports “large quantities”. Removing “large quantities” would make a more defensible statement.

Agreed, “large quantities” was removed.

Line 381: Was the timing of the transport ever specifically discussed or provided?

It was not originally, but we checked how far back the trajectories passed over the fire region (2 – 3 days). We now state this on line 407.

Figure 4: Provide wavelength corresponding to AOD on this and subsequent figures.

Done, but only for the first figure since the captions of the subsequent figures refer to the first.

Figures 7-13: See comment in text

Fixed.

Figure 14(a,b) and 15(a,b): Consider zooming in over North America.

We wanted to show that dust and smoke were indeed enhanced over the entire footprint of what CALIPSO observed for that transect (i.e., relative to a much larger scale). Thus, we did not zoom in on North America.

Figure 18: Adding symbols would help with the error bars. As they are it is hard to tell which pair of upper and lower bars correspond to a single data point.

Done. We also want to note that we restricted our XRF analysis from 27 Aug – 2 Sep due to the strange spike in concentrations on 26 Aug. After closer examination, we realized the data are likely not reliable on that day due to instrumental complications with temperature.

Figure 19: Add (a)-(e) in the caption. Consider changing “small PM2.5” and “large PM2.5” to “low” and “high”.

Done.

Reviewer #2

The manuscript presents an observation-based analysis of Colorado air quality impacted by long range transport of smoke particles from 2015 Pacific Northwest fires. Overall, the analysis is semi-quantitative at most; no transport modeling work is done, nor source-receptor relation is established with robustness. Synoptic chart and satellite data are used together to show the smoke transport pathways, but no new knowledge gained here. The manuscript argues that there is significant dust associated with smoke plume, but again, no figures to show where and when dust are uplifted. Can the dust be from great plains (such as west Nebraska) and not from fire region? it is a very interesting idea that biomass burning can uplift dust and such dust can transport with smoke plumes. The manuscript needs to show more quantitative supports for this idea, either from analysis, modeling, or combined. Strong wind will uplift the soil dust, regardless. Specific concerns are listed below.

We understand the reviewer’s concern, but disagree that more a quantitative analysis is needed. The focus is on the fact that dust is uplifted with the smoke and transported to the Front Range, where it was detected and impacted air quality. Directly showing the dust transport with the smoke is indeed a novel observation, particularly for this region as it has mostly been shown to occur in the dust belt region as we state in the introduction. Additionally we disagree that modeling is needed; we already provide ample evidence for our conclusions (i.e., multiple in situ measurements over the entire Front Range, remote sensing data from two different satellites and a lidar in Boulder, HYSPLIT air mass modeling analysis, in situ wind profiler data, and meteorological reanalysis fields).

We show direct evidence that the dust was transported with the smoke via CALIPSO and state that we evaluated CALIPSO in the surrounding regions to exclude trans-Pacific transport or other regional sources. We also use the meteorological data (e.g., the RAP and wind profiler analyses) and modeled HYSPLIT trajectories to support the sources of the air masses, which as the figures show, were likely not the Great Plains. However, we did include a more statistical HYSPLIT analysis to demonstrate that the fire plume regions indicated by MODIS data was indeed the major source (i.e., transport was dominant from these regions). See response to comment 5 for more details.

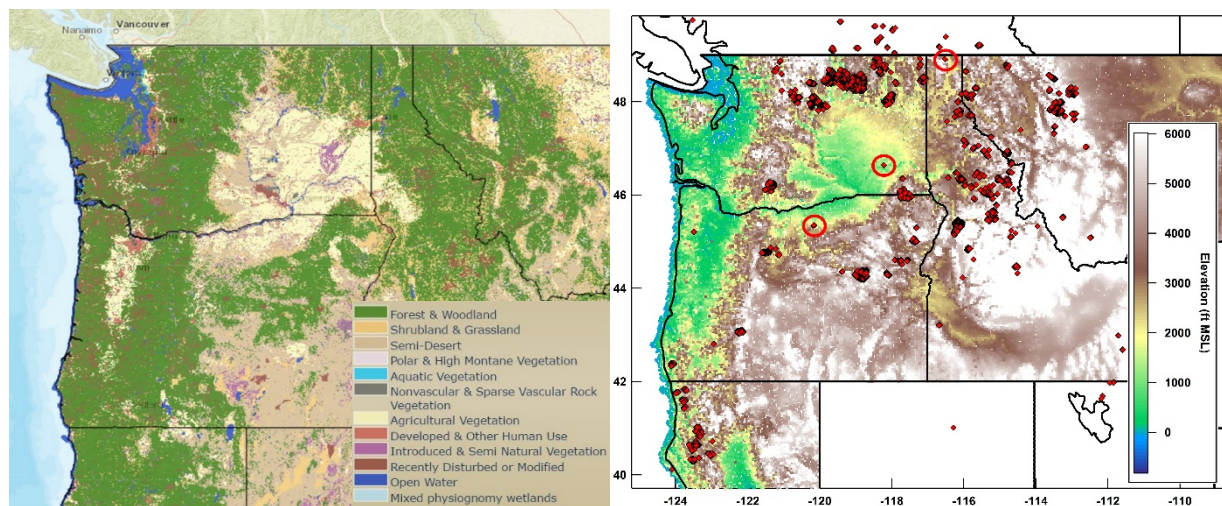
1. The manuscript’s abstract and introduction gives readers an impression that the subject of the study is forest fires. But, in fact, in many cases, the fires studied here are fires in agricultural areas (section 3.2). During the study time period, how much percentage of fires are from forest fires? This question is important because forest fires normally are bigger, inject smoke particles higher into the atmosphere for long range transport. Agricultural fires are smaller and don’t injection smoke particles into the middle troposphere, but smoke particles from these fires can still transport in long distance and can be uplifted into the middle part of the atmosphere during the transport process. Together with the following papers, these points should be discussed either in the introduction or in the section 3.2 and 3.3.

Peterson, D., E. J. Hyer, and J. Wang, 2014: Quantifying the potential for high-altitude smoke injection in North American boreal forest using the standard MODIS fire products and sub-pixel-based methods, *J. Geophys. Res. Atmos.*, 119, 3401-3419.

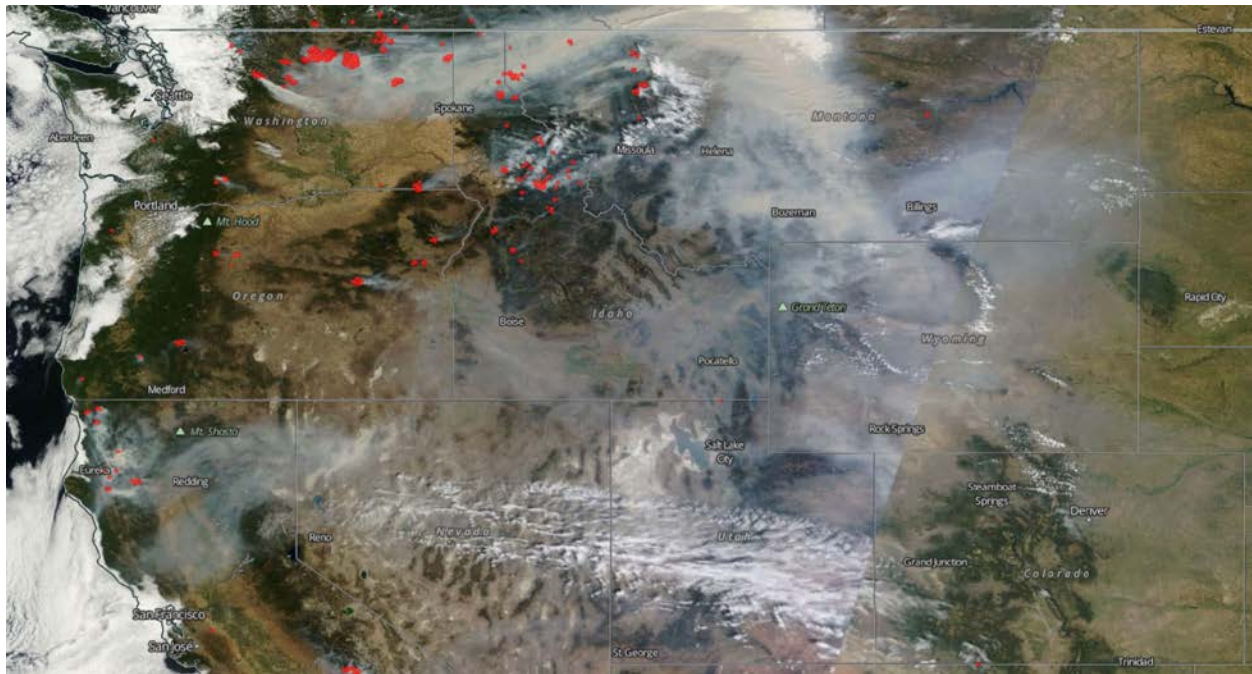
Colarco, P. R., M. R. Schoeberl, B. G. Doddridge, L. T. Marufu, O. Torres, and E. J. Welton, 2004: Transport of smoke from Canadian forest fires to the surface near Washington, D.C.: Injection height, entrainment, and optical properties, *J. Geophys. Res.*, 109, D06203, doi:10.1029/2003JD004248.

Wang, J., S. A. Christopher, U. S. Nair, J. S. Reid, E. M. Prins, J. Szykman, and J. L. Hand, 2006: Mesoscale modeling of Central American smoke transport to the United States: 1. "Top-down" assessment of emission strength and diurnal variation impacts, *J. Geophys. Res.*, 111, D05S17, doi:10.1029/2005JD006416.

The images below show a map containing the most recent USGS land cover types (http://gis1.usgs.gov/csas/gap/viewer/land_cover/Map.aspx) in the left panel and the thermal anomalies (i.e., fire hotspots) detected by MODIS from the entire duration of the study overlaid on a shaded relief map (right panel). It is clear that most of the fires, with the exception of a few in north-central Washington, were located at high elevations and in forested areas. The fires in north-central Washington occurred on high elevation shrub and grassland, which we already state is a land type where fires were observed in the manuscript at the beginning of section 3.2. Almost no fires occurred on agricultural land, with the exception of a couple circled in the right panel. We incorporated this information into a supplementary figure (Figure S1) to support our statement in section 3.2.



Additionally, MODIS shows smoke transported from the fire hotspots, indicating an abundant fuel source to promote evolution of a dense smoke plume. For example, the image below contains MODIS corrected reflectance (true color) and thermal anomalies from 20 Aug. Smoke originating from these fires is prominent and travelled eastward towards the mountain states. The remaining days looked similar (see <https://worldview.earthdata.nasa.gov/>). Thus, the smoke was injected at altitudes where it could be transported long distances, and due to the apparent density of the smoke, were formed from sufficient fuel sources, such as forests.



Even though the fires we observed were predominantly from forested regions, and did indeed inject smoke plumes high enough into the atmosphere such that they were transported long distances, to encompass the fact that a couple of the fires detected during the study time period were from agricultural land, the first sentence of our introduction already stated, "Wildfires in both forested and agricultural regions serve as a steady source of pollutants into the atmosphere." We also now provide additional discussion and some of the references provided by the reviewer in the introduction on lines 41-44 regarding the fire size and injection height.

2. Line 46-47. Smoke particles not only affect clouds - so called indirect effect. They also have a semi-direct effect that affect cloud and atmospheric lapse rate through absorbing aerosols. In particular, when absorbing aerosols are above clouds, the semidirect effect can be enhanced.

Ge, C., J. Wang, and J. S. Reid, 2014: Mesoscale modeling of smoke transport over the Southeast Asian Maritime Continent: coupling of smoke direct radiative feedbacks below and above the low-level clouds, *Atmos. Chem. Phys.*, 14, 159-174.

Thank you for bringing this to our attention. We now discuss this and added the reference on lines 52-53.

3. The paper used K and S as marker for biomass burning particles. However, it is good to use non-soil K instead of total K, as in Wang et al. (2006) and Kreidenweis et al. (2001). In addition, do biomass burning particles contain Ca, Al, etc.?

Kreidenweis, S. M., L. A. Remer, R. Bruinjtes, and O. Dubovik, 2001: Smoke aerosols from biomass burning in Mexico: Hygroscopic smoke optical model, *J. Geophys. Res.*, 106, 4831-4844.

We calculated non-soil K and soil K and have included these in the new Supporting Information file. We also highlight in the text on lines 361-364 that both non-soil and soil K concentrations were higher during the event time period.

Biomass burning aerosols have been shown to contain metals such as Mg, Al, Ca, Cr, Mn, Fe, Ni, Cu, Zn, but it has been suggested that the biomass may have accumulated metal-containing species that were re-emitted during biomass burning, thus the metals may have originated from other sources, such as dust. Although, the exact sources of these metals in biomass burning aerosols remains unknown. Further, if leached from the ground, it is probable that the concentrations of these metals in biomass burning is negligible compared to those in mineral or soil dust. We now explain this and include the following reference on lines 373-376.

Chang-Graham, A. L., Profeta, L. T. M., Johnson, T. J., Yokelson, R. J., Laskin, A., and Laskin, J.: Case Study of Water-Soluble Metal Containing Organic Constituents of Biomass Burning Aerosol, Environ Sci Technol, 45, 1257-1263, 2011.

4. Figure 18. how do you define relative metal mass concentrations? Relative to what? it should be in the figure caption. Figure 19 can be an interesting figure, but presenting the results in total amount for different species is confusing. More PM_{2.5} of course will have more chemical species. Relative percentage of these species with respect to total PM_{2.5} can be interesting to shown. In addition, any statistically significant test is conducted for panel a, -d. For example, in panel, there are significant variation of soil in small PM_{2.5} that can overlap with variation of soil in large PM_{2.5}.

These are relative to the maximum concentration measured from each species, which we now state in the caption of (now) Figure 12. We did this to enable the increases during influences from the fires to be apparent in all the metals, otherwise metals with generally low concentrations (i.e., K) would be buried near zero relative to metals that are generally higher in concentration (i.e., Si). By showing the relative metal mass in this way, it is clear that each metal we discuss is higher in concentration during fire influences as compared to days with a lesser or no influence from the fires.

It is not necessarily true that more PM_{2.5} will have more of each chemical species; take As and Pb shown in (now) Figure 13, for example. Those metals are lower in concentration when PM_{2.5} is higher. We conducted a statistical significance test for SOIL and PM_{2.5} (t-test: two sample assuming unequal variances) and the differences were statistically significant (t-Stat = 2.23 and t-Critical = 1.67). The metal concentration averages in the other panels were also statistically significant according to the t-test. We now note this in the caption.

5. Line 314. "Dust and smoke from fires extended to 10 km". there is no evidence here that dust are from fires. Synoptic charts and back trajectory analysis show there is a high possibility that dust particles may from western part of Nebraska.

It is evident by the back trajectory analysis that air masses did not travel over Nebraska nor the Great Plains on the worst event days shown in red (see e panels in revised Figures 7, 8, and 9). On occasion, surrounding days did pass over the Great Plains (blue dashed lines), but occurred 5 to 10 days back and prior to passing over the fire plume regions (see MODIS data in Figures 4, 5 ,and 6). Only 5 of the 48 trajectories passed over the Great Plains during Event 1, none during Event 2, and 3 of the 48 during Event 3. Thus, the likelihood that the Great Plains played a major source relative to the region where the fire plumes were located is unlikely based on HYSPLIT statistics (see table below), which we now discuss in section 3.3. We also now point out that Event 2, which was the worst in terms of PM_{2.5} and total-column extinction (Figure 3), also had the most transport from the fire regions. The same relationship holds true to remaining events, i.e., the highest (lowest) % transport, the higher (lower) the PM_{2.5} and extinction.

Event	Date	Total # of trajectories	# of trajectories that passed through fire plumes	% of trajectories that passed through fire plumes	per event	# of trajectories that passed through Plains	% of trajectories that passed through Plains	per event
1	15-Aug	12	1	8%	40%	3	25%	10%
	16-Aug	12	3	25%		2	17%	
	17-Aug	12	6	50%		0	0%	
	18-Aug	12	9	75%		0	0%	
2	20-Aug	12	12	100%	96%	0	0%	0%
	21-Aug	12	12	100%		0	0%	
	22-Aug	12	11	92%		0	0%	
	23-Aug	12	11	92%		0	0%	
3	26-Aug	12	11	92%	85%	3	25%	6%
	27-Aug	12	8	67%		0	0%	
	28-Aug	12	10	83%		0	0%	
	29-Aug	12	12	100%		0	0%	

Additionally, 500 hPa geopotential heights (see a and b panels in Figures 7, 8, and 9) clearly show westerly to northwesterly flow along much of the western U.S. and Colorado, and even in Nebraska, indicating transport from those directions and not from Nebraska. Based on this evidence from modelling and reanalysis, a “high probability” of dust arriving from Nebraska is not likely.

Colorado air quality impacted by long-range transport~~transported~~ aerosol: A set of case studies during the 2015 Pacific Northwest fires

Jessie M. Creamean^{1,2*}, Paul. J. Neiman², Timothy Coleman^{1,2}, Christoph J. Senff^{1,3}, Guillaume Kirgis^{1,3}, Raul J. Alvarez³, and Atsushi Yamamoto⁴

¹University of Colorado at Boulder, Cooperative Institute for Research in Environmental Sciences, Boulder, CO, 80309, USA

²NOAA Earth System Research Laboratory, Physical Sciences Division, Boulder, CO, 80305, USA

³NOAA Earth System Research Laboratory, Chemical Sciences Division, Boulder, CO, 80305, USA

⁴~~HORIBA Instruments Inc., Process and Environmental, Irvine, CA~~~~Process and Environmental, HORIBA, Instruments, Inc., Irvine, CA, 92618, USA~~

Correspondence to: Jessie M. Creamean (jessie.creamean@noaa.gov)

Abstract. Biomass burning plumes containing aerosols from forest fires can be transported long distances, which can ultimately impact climate and air quality in regions far from the source. Interestingly, these fires can inject aerosols other than smoke into the atmosphere, which very few studies have evidenced. Here, we demonstrate a set of case studies of long-range transport of mineral dust aerosols in addition to smoke from numerous forest fires in the Pacific Northwest to Colorado, U.S. These aerosols were detected in Boulder, Colorado along the Front Range using Beta-ray attenuation and energy dispersive X-ray fluorescence spectroscopy, and corroborated with satellite-borne lidar observations of smoke and dust. Further, we examined the transport pathways of these aerosols using air mass trajectory analysis and regional and synoptic scale meteorological dynamics. Three separate events with poor air quality and increased mass concentrations of metals from biomass burning (S and K) and minerals (Al, Si, Ca, Fe, and Ti) occurred due to the introduction of smoke and dust from regional and synoptic scale winds. Cleaner time periods with good air quality and lesser concentrations of biomass burning and mineral metals between the haze events were due to the advection of smoke and dust away from the region. Dust and smoke present in biomass burning haze can have diverse impacts on visibility, health, cloud formation, and surface radiation. Thus, it is important to understand how aerosol populations can be influenced by long-range transported aerosols, particularly those emitted from large source contributors such as ~~forest-wild~~fires.

Keywords. Aerosol transport, air quality, mineral dust, biomass burning, remote sensing, in situ observations

1 Introduction

Wildfires in both forested and agricultural regions serve as a steady source of pollutants into the atmosphere. Gas phase constituents such as methane (CH₄), carbon monoxide (CO), carbon dioxide (CO₂), sulphur dioxide (SO₂) and nitrogen oxides (NO_x; NO + NO₂) can be produced from burning of biofuels (Gadi et al., 2003; Radojevic, 2003), in addition to precursors that induce ozone production (Jaffe and Wigder, 2012). Additionally, wildfires produce large

concentrations of aerosols which are injected into the atmosphere or formed in the smoke plume via secondary processes and include carbonaceous species (elemental and organic carbon) (Park et al., 2003; Spracklen et al., 2007) and biogenic heavy metals (including but not limited to Fe, Mn, Cd, Cu, Pb, Cr, and Ni) (Nriagu, 1989; Radojevic, 2003). Soluble inorganic species such as sulphate, nitrate, ammonium, and chloride are found in fire emissions and partitioned to the particle phase through heterogeneous reactions with the gas phase species released during the combustion process (Pio et al., 2008). Strong, turbulent winds inside combustion zones from controlled and wild vegetation fires can introduce considerable amounts of dust particles into the free troposphere, which can subsequently be transported over thousands of kilometres with the smoke (Clements et al., 2008; Ansmann et al., 2009; Baars et al., 2011). Forest fires tend to be much larger than agricultural fires, and enable injection of smoke high into the free troposphere (Colarco et al., 2004; Peterson et al., 2014). Yet, smoke from agricultural, and shrub and grassland fires can still be transported long distances. However, few studies have documented how wildfires from any of the aforementioned biofuel sources inject mineral dust into the atmosphere (Gaudichet et al., 1995; Chalbot et al., 2013; Yang et al., 2013; Nisantzi et al., 2014), particularly in heavily forested or agricultural regions such as the Pacific Northwest of the U.S. where dust sources are limited relative to arid regions in Africa, the Middle East, and Asia. Prescribed burning (i.e., slash-and-burn techniques) and wildfires are common in these arid “dust belt” regions, inducing the simultaneous emission of dust and smoke (Streets et al., 2003; Pinker et al., 2010).

Aerosols produced directly from wildfires (i.e., carbonaceous and soluble inorganic particulates) or injected into the free troposphere from smoke plume dynamics (i.e., mineral dust) have diverse effects on climate and air quality. For instance, absorbing aerosols such as soot from fires enhance the semi-direct effect that affect cloud and atmospheric lapse rate, particularly when the absorbing aerosols are above cloud (Ge et al., 2014). Further, hygroscopic organic aerosol, sulphate, and nitrate can enable aerosols to serve as cloud condensation nuclei (CCN) (Cruz and Pandis, 1997), whereas mineral dust and black carbon are effective ice nucleating particles (INPs) at sub-freezing temperatures (DeMott et al., 1999; DeMott et al., 2003; Vali et al., 2015). Both of these aerosol nuclei modify cloud radiative properties, lifetime, and impact precipitation formation, and have been shown to originate from prescribed burns and wildfires (Eagan et al., 1974; McCluskey et al., 2014). Enhanced pollutants from fires also severely influence air quality, and can prompt adverse health effects (Bravo et al., 2002; Phuleria et al., 2005; Wiedinmyer et al., 2006). For instance, smoke plumes from wildfires have been linked to childhood mortality (Jayachandran, 2008), asthma (Bowman and Johnston, 2005), and various respiratory illness and diseases (Mott et al., 2002; Moore et al., 2006). These effects are additionally complicated by aging from biogenic gases in the smoke plume during transport. Further, previous air quality studies on the East Coast of the U.S. have shown that enhanced aerosol optical depths associated with both wildfires and anthropogenic sources can cause large errors in meteorological models used to forecast poor air quality events (Zamora et al., 2005). Overall, the aerosol species emitted or formed from wildfire plumes are complex in nature and possess several diverse climate and health effects, thus demonstrating the need to better understand the various types, sources, and transport pathways of these emissions.

Air quality is strongly dependent not only on emission sources such as wildfires, but also on weather and climate change (Jacob and Winner, 2009). Regions with complex topography such as the Front Range of Colorado, U.S. (see Figure 1) have unique meteorological phenomena such as upslope/downslope flows that serve as agents for focusing or cleaning out local air pollution from the Denver metropolitan area (Haagenson, 1979). Typically, this region is characterized by good air quality in terms of particulate matter (PM) relative to other larger urban and industrial areas, although it experiences occasional pollution episodes due to modulation of the mountain slope dynamics, oil and natural gas production, and wildfires (Watson et al., 1998; Sibold and Veblen, 2006; Brown et al., 2013). Here, we show that the Front Range air quality was severely impacted by long-range transported wildfire emissions from the Pacific Northwest during August 2015. A reoccurring influx of ~~pollutants, including SO₂, NO_x, and~~ smoke aerosols, infiltrated the Front Range region due to shifts in regional and synoptic scale meteorology. Interestingly, mineral dust was also transported with the smoke plume to the Front Range from the wildfires. This complex mixture of ~~gases and~~ aerosols can have numerous climate and health effects in the region, and should be evaluated to develop a better understanding of future influences from wildfire emissions, especially considering a warmer and drier climate will potentially lead to more frequent wildfires (Westerling et al., 2006; Liu et al., 2010).

2 Methods

2.1 Satellite observations

The source of aerosols from the fires was determined using imagery from the Moderate Resolution Imaging Spectroradiometer (MODIS) on board the Terra satellite. MODIS is a multi-spectral sensor with 36 spectral bands, ranging in wavelength from 0.4 to 14.2 μm . Aerosol optical depth (AOD) data ~~at 550 nm~~ from MODIS were acquired from the Giovanni data server (<http://giovanni.gsfc.nasa.gov/giovanni/>) for daily AOD at a 1° spatial resolution using a domain of 82°W to 163°W and 26°N to 59°N (MOD08_D3_051). MODIS AOD is retrieved from three spectral channels (0.47 μm , 0.66 μm , and 2.1 μm) using the algorithm described by Kaufman et al. (1997) in cloud-free pixels (10 km x 10 km grid box) (Ackerman et al., 1998). Fire and surface thermal anomaly data were also acquired from the MODIS Terra satellite using brightness temperature measurements in the 4- μm and 11- μm channels (<https://earthdata.nasa.gov/labs/worldview/>) (Giglio, 2010). The fire detection strategy is based on absolute detection of a fire (when the fire strength is sufficient to detect), and on detection relative to its background (to account for variability of the surface temperature and reflection by sunlight) (Giglio et al., 2003). The algorithms include masking of clouds, bright surfaces, glint, and other potential false alarms (Giglio et al., 2003). Swaths from overpasses over the Pacific Northwest were used to determine the locations of fires on a daily basis.

In order to evaluate the types of aerosols present in enhanced AOD plumes over the western U.S., aerosol subtype data were retrieved from Cloud-Aerosol Lidar with Orthogonal Polarization (CALIOP) on board Cloud-Aerosol Lidar and Infrared Pathfinder Satellite Observations (CALIPSO). Level-2 ValStage1 V.30 Vertical Feature Mask data obtained from NASA's Earth Observing System Data and Information System (EOSDIS; <https://search.earthdata.nasa.gov/>) contain vertically-resolved data of aerosol layer sub-type, including but not limited

105 to smoke, dust, and polluted dust (i.e., dust mixed with smoke) (Vaughan et al., 2004; Omar et al., 2009; Winker et
106 al., 2009). CALIPSO was launched on 28 Apr 2006 and flies in an orbital altitude of 705 km as part of the sun-
107 synchronous “A-train” satellite constellation. CALIOP is an elastic backscatter lidar operating at 532 nm and 1064
108 nm, completed with a depolarization channel at 532 nm to enable detection of aerosols and clouds. Granule data were
109 acquired from orbital swaths that passed over the north-western U.S. (domain includes Washington, Oregon, northern
110 California, Idaho, Nevada, Montana, Wyoming, Utah, and Colorado) from 15 Aug to 2 Sep 2015 and processed using
111 modified Python code developed by the Hierarchical Data Format (HDF) group at the University of Illinois, Urbana-
112 Champaign (<http://hdfeos.org/>). Aerosol sub-types were also examined off the U.S. West Coast across the central
113 North Pacific Ocean, in the context of air mass trajectory analysis, to ensure mineral dust and smoke were transported
114 to Colorado from the Pacific Northwest fires rather than from deserts or fires overseas.

115 2.2 Colorado air quality data

116 All air quality data were acquired from the Colorado Department of Public Health and Environment (CDPHE;
117 <http://www.colorado.gov/airquality/report.aspx>) from 15 Aug to 2 Sep 2015 at various sites throughout the Colorado
118 Front Range (see Figure 1). ~~Table 1 provides the site latitudes, longitudes, elevations, and which measurements were~~
119 ~~available at each site.~~ ~~The DESCI site (Denver Visibility Station; 39.73°N, 104.96°W; 1,633 m MSL) is highlighted~~
120 ~~in blue, near downtown Denver, where horizontal total-column atmospheric extinction (km^{-1}) data measured with a~~
121 ~~transmissometer are available through CPDHE. These data provide a quantitative measure of “haziness” indicated~~
122 ~~throughout the text. Table 1 provides the site latitudes, longitudes, elevations, and which PM measurements were~~
123 ~~available at each site.~~ ~~Table 1 provides the site latitudes, longitudes, elevations, and which measurements were~~
124 ~~available at each site.~~ Hourly measurements included mass concentrations ($\mu\text{g m}^{-3}$) of particulate matter for particles
125 with diameters $\leq 2.5 \mu\text{m}$ ($\text{PM}_{2.5}$) and $\leq 10 \mu\text{m}$ (PM_{10}). ~~Carbon monoxide (CO), sulphur dioxide (SO_2), nitric oxide~~
126 ~~(NO), nitrous oxide (NO_2), and ozone (O_3) were also evaluated but no significant differences were observed between~~
127 ~~haze and non-haze time periods, thus the data are not presented.~~ All times shown are coordinated universal time [UTC;
128 local time or mountain daylight time (MDT) + 6].

129 2.3 In situ aerosol observations at Boulder, Colorado

130 Real-time, hourly ambient aerosols samples were analysed for $\text{PM}_{2.5}$ ~~total~~-mass concentrations ($\mu\text{g m}^{-3}$) and
131 concentrations of various metals (ng m^{-3}) using the HORIBA, Ltd. PX-375 continuous particle mass and elemental
132 speciation monitor ([http://www.horiba.com/process-environmental/products/ambient/details/continuous-particulate-](http://www.horiba.com/process-environmental/products/ambient/details/continuous-particulate-monitor-with-x-ray-fluorescence-px-375-27871/)
133 [monitor-with-x-ray-fluorescence-px-375-27871/](http://www.horiba.com/process-environmental/products/ambient/details/continuous-particulate-monitor-with-x-ray-fluorescence-px-375-27871/)) from 26 Aug to 2 Sep 2015 at the National Oceanic and
134 Atmospheric Administration (NOAA) David Skaggs Research Centre (DSRC) located in Boulder, Colorado (39.99°N,
135 105.26°W, and 1672 m MSL; see Figure 1). The PX-375 draws in air at 16.7 L min^{-1} through a U.S. Environmental
136 Protection Agency (EPA) Louvered PM_{10} inlet, then subsequently passes through a BGI Very Sharp Cut Cyclone
137 (VSCC™) to filter for particles smaller than $2.5 \mu\text{m}$ in diameter. Air is pulled through a nozzle for 60 minutes per
138 hourly sample, where particles are subsequently deposited in a 100-mm diameter spot on Teflon™ PTFE fabric filter
139 tape for analysis. Once the sample is collected for 60 minutes, beta-ray attenuation and energy dispersive X-ray

Field Code Changed

fluorescence spectroscopy (EDXRF) analyses are conducted for 60 minutes and 1000 seconds, respectively, per hourly sample, simultaneous to the [sampling collection](#) of the subsequent sample. Beta-ray attenuation analysis is used to measure total PM_{2.5} mass concentrations and EDXRF is used to analyse concentrations of Ti, V, Cr, Mn, Fe, Ni, Cu, Zn, As, Pb, Al, Si, S, K, and Ca. The EDXRF unit contains a CMOS camera for sample images. Calibration material used for X-ray intensity is NIST SRM 2783. Lower detection limits (LDLs) are shown in Table 2 and error was calculated to be $\pm 2\%$ for hourly metal concentrations. Hourly total PM_{2.5} mass concentrations had an LDL of 2.00 $\mu\text{g m}^{-3}$.

2.4 Aerosol and ozone remote sensing observations at Boulder, Colorado

The Tunable Optical Profiler for Aerosol and oZone (TOPAZ) lidar was operated at the DSRC on 9 days from 14 Aug through 2 Sep 2015 and it collected about 62 hours of ozone and aerosol profile data, primarily between mid-morning and early evening local time. TOPAZ is a state-of-the-art, tunable ozone differential absorption lidar. It emits pulsed laser light at three ultraviolet wavelengths between 285 and 295 nm and measures ozone as well as aerosol backscatter and extinction profiles with high temporal and spatial resolutions (Alvarez et al., 2011). The TOPAZ lidar is mounted in a truck with a rooftop two-axis scanner. This scanner permits pointing the lidar beam at elevation angles between -5 and 30 degrees at a fixed but changeable azimuth angle. To achieve zenith operation the scanner mirror is moved out of the beam path. Typical TOPAZ operation consists of a scan sequence at 2, 6, 20, and 90 degrees elevation, repeated approximately every five minutes. The range-resolved ozone and aerosol observations at the shallow elevations angles are projected onto the vertical and spliced together with the zenith observations, resulting in composite vertical ozone and aerosol profiles from about 15 m to 2–3 km above ground level (AGL) at five minutes time resolution (Alvarez et al., 2012). In this study, we only used the lidar aerosol extinction profiles measured at a wavelength of 294 nm. The aerosol profile retrieval requires assumptions about the lidar calibration constant and the aerosol extinction-to-backscatter or lidar ratio. For this study we used an altitude-constant lidar ratio of 40 sr, which is a good approximation for continental and urban aerosols. The lidar signal at the aerosol wavelength of 294 nm is also affected by ozone absorption. Therefore, uncertainties in the ozone observations can cause biases in the aerosol retrieval. This, combined with uncertainties in the calibration constant and lidar ratio, can lead to errors in the aerosol extinction coefficient profiles of up to about 30%. The precision of the 5-minute aerosol extinction measurements is typically better than 10%.

2.5 Meteorological data and analysis

A gridded perspective of synoptic-scale conditions across North America was provided using the NOAA/National Centres for Environmental Prediction (NCEP) Rapid Refresh numerical data package [RAP; <http://rapidrefresh.noaa.gov/> (Benjamin et al., 2016)]. The RAP is an operational assimilation/modelling system updated hourly, with 13-km horizontal resolution and 50 vertical levels.

Air mass backward trajectory analyses were conducted using HYSPLIT 4 (Draxler and Rolph, 2011) and data from the NOAA/NCEP Global Data Assimilation System (GDAS) (Kalnay et al., 1996). HYSPLIT trajectories do not

include processes that may affect particle concentrations such as convective transport, wet removal, or dry removal, and are only intended to highlight the possible transport pathways. To study the potential for transport from the Pacific Northwest fires region, and to eliminate potential contribution from aerosol sources overseas, we used an ensemble of backward trajectories initiated at multiple altitudes and times ending above the NOAA building in Boulder. Ten-day back trajectories were initiated every 6 hours (at 00:00, 06:00, 12:00, and 18:00 UTC) during 15 Aug–2 Sep 2015 at 500, 1000, and 2000 m AGL (corresponds to 2172, 2672, and 3672 m MSL).

A 449-MHz wind profiler (White et al., 2013), deployed near the Boulder Atmospheric Observatory in Erie, Colorado (BAO; 40.05N, 105.01°W, and 1577 m MSL; location shown in Figure 1), provided hourly-averaged profiles of horizontal wind. The high (low) mode extended from 145 m (195 m) to 10074 m (5059 m) AGL with a vertical resolution of 200 m (100 m). The wind-profiler data were edited objectively using the vertical-temporal continuity method of Weber et al. (1993) and then subjected to additional manual editing as needed. For the purpose of this study, we utilized only the low-mode observations.

3 Results and discussion

3.1 Haze events induced poor air quality along Colorado's Front Range

The shift in air quality was evident during three August haze events in the Denver metro area. Figure 2 shows photos of notable air quality transitions in Denver looking westward towards the foothills of the Rocky Mountains and Figure 3 shows the ~~total-column~~ atmospheric extinction measurements from DESC. Higher values of extinction indicate hazier conditions. The image on 15 Aug shows typical, clean conditions, where the foothills were visible west of Denver. Extinction was also relative low on 15 Aug. On 17 Aug, a haze settled in the region, creating a low-level pollution plume that masked the view of the foothills. This haze continued to infiltrate the Denver metro area, reaching the poorest visibility (i.e., highest extinction) on 23 Aug. This haze persisted in the Denver metro area until 27 Aug, when clear conditions were re-established and the foothills were once again visible. However, the air quality deteriorated ~~once~~ again by 29 Aug, with hazy conditions obscuring the foothills. This haze event was shorter lived, clearing out ~~once again~~ on 31 Aug. The cleaner conditions persisted until the end of the measurement period on 2 Sep. The qualitative observations of the three separate haze events were corroborated by in situ air quality measurements along the Front Range. Figure 3 also shows hourly and daily averaged $PM_{2.5}$ mass concentrations (herein, simply called “ $PM_{2.5}$ ”) at the sites provided in Table 1. Overall, three separate haze events occurred along the Front Range with the worst days visually observed (Figure 2) on the 17, 23, and 29 Aug (events 1, 2, and 3, respectively), when extinction was highest, $PM_{2.5}$ reached maximum concentrations, and a cold front passed through (discussed in section 3.3). Prior to each of these events, $PM_{2.5}$ was suppressed then slowly increased to each event's maximum concentrations on 17, 23, and 29 Aug. $PM_{2.5}$ slowly decreased following each of these haze events. PM_{10} (not shown) did not follow similar increases and decreases as the $PM_{2.5}$, suggesting the smaller particles contributing to $PM_{2.5}$ originated from different, likely more distant sources as compared to coarser particles contributing to the PM_{10} , which are likely from more local sources (VanCuren, 2003; Neff et al., 2008).

3.2 Biomass burning plume propagates towards Colorado

During the 15 Aug–2 Sep time period, fires in high elevation (>3000 feet MSL) ~~both-forested and-agricultural~~ vegetation-areas and to some extent in shrub and grasslands in the Pacific Northwest were prominent, while few fire hotspots were located in low elevation agricultural land (see Figure S1 of the Supporting Information). Figures 4–6 show MODIS retrievals of fire hotspots and aerosol optical depth (AOD) during the first, second, and third haze events in Colorado, when numerous fires were detected in Washington, Oregon, northern California, northern Idaho, and north-western Montana. Three cases are defined as the time periods surrounding and including the haze event days: Case 1 (15–18 Aug), Case 2 (20–23 Aug), and Case 3 (26–29 Aug).

On 15 Aug, prior to the onset of the first haze event in Colorado, the plume of enhanced AOD propagating from the fires in the Pacific Northwest remained north of Colorado in Montana and southern Canada (Figure 4~~Figure-4~~). The air above the Denver/Boulder area contained relatively diminished AOD (0.12, averaged from the domain of 39.5°N, 104.5°W, 40.5°N, and 105.5°W). Although the core of the plume remained north of Colorado, its more diffuse southern region drifted south-eastward on 16 Aug. By 17 Aug, enhanced AOD was observed along the Front Range in northcentral Colorado near Denver/Boulder (0.37). The AOD slightly decreased on 18 Aug over Denver/Boulder (0.25), which is supported by the decrease of $PM_{2.5}$ starting on 18 Aug from the CDPHE data (Figure 3~~Figure-3~~). AOD increased in value and spatial extent on 20 Aug during the second haze event, when more fires were detected in the Pacific Northwest (see increase in number of MODIS hot-spots in Figure 5~~Figure-5~~). This plume contained a high density of aerosols that travelled over the northcentral U.S. The southern periphery of this plume impacted Colorado east of the Continental Divide starting on 20 Aug, as corroborated by the CDPHE air quality measurements in Figure 3~~Figure-3~~. Although the AOD values were not as enhanced over Colorado as compared to the core of the AOD plume, AOD values over the Front Range were enhanced as compared to before the long-range transport of this plume. Enhanced AOD was observed around Denver/Boulder and the Front Range the following three days (0.26–0.35), with the largest values in this four-day period observed on 23 Aug. The third haze event (Figure 6~~Figure-6~~) followed a similar evolution to the first two. The AOD plume remained north of Colorado on 26–27 Aug, then infiltrated the northern and eastern part of the state on 28–29 Aug. The AOD values over Denver/Boulder during this event (0.26–0.45) were considerably larger than the two previous events. It is important to note that AOD is a column measurement, thus the largest aerosol concentrations may be elevated in the atmosphere as compared to what is observed on the ground. However, the AOD observations still provide information regarding the spatial extent of the plume of aerosols emitted from the fires and that Colorado was indeed impacted by air transported from the Pacific Northwest fires.

Further, the satellite retrievals generally corroborate the air quality observations on the ground along the Front Range in terms of when large concentrations of aerosols might be expected. More fires were detected across the Pacific Northwest by MODIS during the second event (678 fires, on average) when $PM_{2.5}$ was largest as compared to the first event (231 fires, on average), which had the smallest maximum $PM_{2.5}$ out of the three haze events. The third event had $PM_{2.5}$ values in between the first and second, while also having 607 fires on average. Thus, the number of fires

likely influenced the relative amount of smoke produced and transported to the Front Range. However, meteorological conditions as described below also played a vital role in enabling transport of the smoke.

3.3 Synoptic and regional scale meteorology fuel long-range aerosol transport from the Pacific Northwest

The transport of the enhanced AOD plume from the Pacific Northwest to Colorado during each of the three events, and the relationship between the AOD column and ground-based in situ observations, are supported by the meteorological features present on both the synoptic and regional scales. Plan-view synoptic analyses aloft and at the surface during the first air quality event along Colorado's Front Range on 17–18 Aug 2015 are shown in Figure 7. At 500 hPa (Figure 7a and [eb](#)), a transient shortwave trough embedded in baroclinic zonal flow aloft migrates eastward across the northern Rocky Mountains (i.e., north of Colorado), with westerly (north-westerly) flow preceding (following) the passage of the trough axis. These flow patterns are corroborated by the HYSPLIT air mass back trajectories during the first event, shown in [Figure 7f](#)[Figure 8a](#). [On average, air mass back trajectories passed over the fire plume region 40% of the time, i.e., 19 of the 48 trajectories passed over regions of enhanced AOD and fire hotspot locations from MODIS.](#) At the surface, high pressure and shallow cool air initially resides primarily north of Colorado at 0600 UTC 17 Aug ([Figure 7b](#)[Figure 7c](#)). However, by 2100 UTC 17 Aug (Figure 7d), the shallow cool air has moved southward across eastern Colorado. A companion time-height section of hourly wind profiles at BAO ([Figure 7f](#)) shows low-level southerly flow ahead of the frontal passage at ~1100 UTC 17 Aug and generally westerly to northwesterly flow aloft for the duration of the plot. The observed flow aloft is represented in many of the back trajectories, which show west to northwest flow reaching Boulder during this event. Following the frontal passage at the wind profiler, the shallow cool air mass deepens to ~3 km MSL by 1800 UTC 17 Aug in generally northerly-component flow. Thereafter, the depth of the cool air decreases as the low-level flow shifts to south-easterly. Operational rawinsonde data from Denver (not shown) captures the top of the frontal inversion at 2.1 km MSL at 1200 UTC 17 Aug and at 2.7 km MSL at 0000 UTC 18 Aug, consistent with the wind-profiler analysis of the time-varying frontal altitude at BAO. For plan-view context, the times of the synoptic analyses are marked on the time-height section. The [large-high](#) PM_{2.5} values ([Figure 3](#)[Figure 3](#)) on 17 Aug are corroborated by the transition of air arriving from enhanced AOD regions (see air mass backward trajectories in [Figure 7e](#)[Figure 8a](#)) over and off the coast of the Pacific Northwest and northern California ([Figure 4](#)[Figure 4c](#)). PM_{2.5} increased markedly after the passage of the shallow front, thus suggesting the post-frontal air mass—which originated over Wyoming downstream of the Pacific Northwest fires—contains a large concentration of particulates from those fires.

The evolution of the shallow cold front described above is typical of southward propagating cold fronts more generally across eastern Colorado, and the frontal propagation is influenced heavily by the complex regional topography depicted in [Figure 1](#)[Figure 4](#). Specifically, the blocking effect of the Rocky Mountains accelerates cold air southward along the eastern side of the high terrain (e.g., Colle and Mass, 1995; Neiman et al., 2001). Additionally, the postfrontal northerly-component airstream flowing across the west-east-oriented Cheyenne Ridge in south eastern Wyoming induces an anticyclonic gyre to the lee (south) of this ridge, subsequently shifting the postfrontal flow from northerly to easterly and driving the front westward against Colorado's Front Range (e.g., Davis, 1997; Neiman et al., 2001).

282

283 The meteorology during the second air quality event, on 22–23 Aug (Figure 8Figure-10), is qualitatively similar to
 284 its predecessor, although the transient shortwave trough aloft is more amplified during the latter event (Figure 8Figure
 285 40a and eb). Consequently, during the second event, the terrain-trapped cold front and its trailing shallow cool air
 286 mass east of the Rockies surges much farther southward across eastern New Mexico (Figure 8Figure-10bc and d). The
 287 corresponding air mass back trajectories (Figure 8Figure-8be) traveled south-eastward from the Pacific Northwest
 288 fires to Colorado and passed over the fire plume region 96% of the time, leading to the worst event along the Front
 289 Range in terms of $PM_{2.5}$ and total-column extinction (Figure 3).–The wind-profiler analysis at BAO (Figure 8Figure
 290 44) shows an abrupt low-level wind shift from westerly to easterly with the frontal passage at 1900 UTC 22 Aug,
 291 followed by a rapid deepening of the shallow cool air mass to nearly 3 km MSL. Thereafter, the depth of this air mass
 292 ranges between ~2.2 and 3.4 km MSL. Nearby rawinsonde observations at Denver from 0000 UTC 23 Aug to 0000
 293 UTC 24 Aug (not shown) document a strong frontal inversion ranging between 3.3 and 3.8 km MSL, consistent with
 294 the wind-profiler analysis. Above the shallow cool air mass, the profiler shows westerly flow aloft, shifting to north-
 295 westerly with the passage of the transient shortwave trough. The largest $PM_{2.5}$ values observed during this event, on
 296 23 Aug, corresponds to the most direct transport of air (Figure 8Figure-8be) from over the enhanced AOD regions
 297 over the Pacific Northwest fires (Figure 5Figure-5). As with the previous case, the $PM_{2.5}$ increased markedly with the
 298 passage of the shallow front (Figure 3Figure-3). Significantly, air quality is considerably poorer with the second event,
 299 perhaps due partly to a stronger cold-frontal push across Colorado’s Front Range that originated near the smoke
 300 source region and partly due to north-westerly (rather than westerly) flow aloft that could transport the smoke through
 301 a deeper layer toward Colorado. Further, more fires were detected during the second event (678, on average) compared
 302 to the first event (231 fires, on average), thus the larger number of fires could result in more smoke production and
 303 thus a denser smoke plume transported to the Front Range.

304

305 The synoptic-scale conditions on 27–28 Aug (Figure 9Figure-12) associated with the third air quality case differ
 306 significantly-considerably from those of the two earlier events. Most significantly, a broad ridge aloft covers the
 307 intermountain West for the duration of this final event, while an embedded weak shortwave trough migrates eastward
 308 through the ridge from Wyoming/Colorado to the Great Plains (Figure 9Figure-12a and eb). A surface reflection of
 309 the upper-level shortwave trough is manifest as a weak low-pressure centre over western Nebraska and Kansas at 1800
 310 UTC 27 Aug (Figure 9Figure-12bc). This low migrates eastward during the subsequent 24 h (Figure 9Figure-12d) in
 311 tandem with the upper-level shortwave. Because this surface low resides beneath a mean ridge aloft, the temperature
 312 contrast across this trailing cold front is weaker than its earlier counterparts (not shown). Nevertheless, the southward
 313 migration of the front east of the Rockies suggests that terrain blocking may have influenced its evolution. The air
 314 mass back trajectories show parcels originating from the region of the fires and enhanced AOD 85% of the time,
 315 similar to the trajectories from the earlier two events (Figure 9e).– Companion observations from the BAO wind
 316 profiler (Figure 9Figure-13) capture the shallow frontal passage at 2000 UTC 27 Aug, when westerly flow shifts
 317 abruptly to northerly. Above 3 km MSL, the wind field exhibits a more gradual transition from westerly to north-
 318 westerly as the weak shortwave trough moves across the wind profiler. The Denver rawinsondes at 0000 and 1200

UTC 28 Aug observed a frontal inversion at ~2.1 km MSL (not shown). It is less prominent than the frontal inversions during the earlier events, largely because the temperature contrast across this front is weaker than its predecessors. The subsequent rawinsonde profile at 0000 UTC 29 Aug (not shown) captures a deep, dry-convective boundary layer extending up to 4 km MSL, despite persistent low-level northerly flow. Sensible heating eroded the remnant low-level cool air east of the Rockies. PM_{2.5} increases following the initial shallow cold-frontal passage at 2000 UTC 27 Aug and continues to increase for the remainder of the wind-profiler time-height section, as deep northerly-component flow behind the weak shortwave trough transports smoke particulates across Colorado.

3.4 Mineral dust and smoke arrive along the Front Range

The types of aerosols present in the enhanced AOD plumes that were transported towards the Front Range via the aforementioned synoptic conditions were evaluated using additional satellite-based measurements and support the interpretation of transport of aerosols from the wildfires in the Pacific Northwest to Colorado. ~~Figure 10~~Figures 14–16 shows aerosol subtype data from the CALIPSO satellite in planar (a panels) and vertical-profile (b panels) views during Event 1. CALIPSO data were strikingly similar for Events 2 and 3 and are provided in the Supporting Information. Only on the day prior to, or on the worst day of, each haze event are shown, although aerosol subtype data were examined anytime CALIPSO passed over the Pacific Northwest or Colorado from 15 Aug to 2 Sep. CALIPSO demonstrates the presence of smoke, dust, or polluted dust (dust mixed with smoke in each profile) during times that intersect the enhanced AOD plume propagating from the Pacific Northwest or when over Colorado. Dust and smoke plumes from the fires extended up to 10 km MSL over the western U.S. The mineral dust and smoke detected by CALIPSO in transit to the Front Range was also detected with the TOPAZ lidar and the in situ aerosol particle mass and speciation monitor at the DSRC. ~~Figure 11~~ Figure 17 shows aerosol extinction profiles from the surface to 2.5 km AGL measured with the TOPAZ lidar on 9 days during the smoke episodes. The time resolution of the extinction profiles is 5 minutes and the vertical resolution is 1 m at the lowest altitudes, increasing to 6 m above 500 m AGL. The observations on 14 Aug and 2 Sep, which bracket the smoke episodes, indicate very clean conditions with AOD from the surface up to 2.5 km AGL (AOD_{2.5km}) of 0.05 and 0.04, respectively. ~~These clean days indicated by TOPAZ agree with the extinction data from DESCI (i.e., low extinction values were observed these days:).~~ Aerosol extinction coefficients and AOD_{2.5km} were significantly larger during the smoke episodes with an approximately 7-fold increase in AOD_{2.5km} on 20 and 21 Aug. ~~This time period also corresponds to increasing extinction at DESCI (Figure 3).~~ Aerosol extinction was enhanced over the entire 2.5 km column, but the largest aerosol extinction values were observed in the boundary layer in the lowest few hundred meters up to 1.5 km AGL. Also, the lidar measurements reveal that on most days aerosol extinction varied significantly over the course of the day (e.g., 20 Aug). The largest aerosol extinction values around 1–1.5 km AGL observed on 19 Aug were primarily due to swelling of aerosol particles in the moist relative humidity environment beneath cumulus clouds at the top of the boundary layer. However, aerosol extinction in the lower part of the boundary was still significantly larger than on 14 Aug, which is consistent with the larger aerosol particle concentrations in the smoke plumes. The lidar measurements are consistent with the ~~atmospheric column total extinction measurements from DESCI, and the~~ in situ PM_{2.5} and MODIS AOD observations. When comparing lidar AOD_{2.5km} with MODIS AOD one has to be cognizant of the fact that the TOPAZ

observations only cover a portion of the atmospheric column and that the two AOD measurements were made at different wavelengths. [A comparison between the near-surface TOPAZ and DESCI extinction observations also needs to take into account that the measurements were made at different wavelengths.](#)

~~Figure 12~~[Figure 18](#) shows the time series of $PM_{2.5}$, soil mass concentrations, and elemental mass concentrations (data from the PX-375 was not available prior to this time period due to instrumental complications). Soil concentrations were calculated by following the Interagency Monitoring of Protected Visual Environments (IMPROVE) convention using concentrations of specific metals: $SOIL = 2.2[Al] + 2.49[Si] + 1.63[Ca] + 2.42[Fe] + 1.94[Ti]$ (Malm et al., 1994; Hand et al., 2011). Both $PM_{2.5}$ and soil mass concentrations increased during the worst haze event days (i.e., 26 and 29 Aug), when the Pacific Northwest fires were influencing air along the Front Range and when CALIPSO showed the presence of smoke and dust over the western U.S. The diurnal pattern is likely caused by the upslope/downslope flow patterns due to proximity from the base of the foothills, which is particularly pronounced in the summer (Toth and Johnson, 1985). Further, select metals also increased in concentrations during haze events, particularly those typically sourced from mineral dust (i.e., in the IMPROVE soil convention equation) and S and K, which are metal tracers that have been observed in smoke or biomass burning aerosols originating from fires (Artaxo et al., 1994; Gaudichet et al., 1995; Yamasoe et al., 2000; Pachon et al., 2013). [It is important to note that K may also originate from soil. We calculated the soil K and non-soil K based on the methods of Kreidenweis et al. \(2001\), which is shown in the Supporting Information. Concentrations of both soil K and non-soil K were highest during the influence from the fires. Additionally, IMPROVE measurements at the Rocky Mountain National Park location showed higher concentrations of soil, S, and K during event days in August, corroborating our measurements \(see Supporting Information\).](#)

~~Figure 13~~[Figure 19](#) shows the average concentrations of mineral dust or biomass burning metal tracers from the PX-375 from 26 Aug to 2 Sep, during conditions influenced by the Pacific Northwest fires (days with enhanced $PM_{2.5}$; 29–30 Aug) and days with cleaner, normal Front Range conditions (days with ~~small-low~~ $PM_{2.5}$; remaining days during this time period). $PM_{2.5}$ and soil mass, biomass burning metals (S and K), and mineral dust marker (Al, Si, Fe, and Ca) concentrations were all larger, on average, during influences from the Pacific Northwest fires, corroborating the CALIPSO observations. [It is important to note the possibility that some small concentration of Ca, Al and Fe could also originate from biomass burning, although the apportionment of this source remains in question and their contribution from biomass burning aerosol are likely minor in comparison to their concentrations in mineral dust \(Chang-Graham et al., 2011\).](#) Also included are metals that are typical of industrial tracers As and Pb (~~Figure 13~~[Figure 19e](#)) (Paciga and Jervis, 1976; Hutton and Symon, 1986; Thomaidis et al., 2003), which were actually ~~smaller-lower~~ [in concentration](#) during influences from wildfires and ~~larger-enhanced~~ during normal, regionally-sourced influences. The average $PM_{2.5}$ mass concentration from the CDPHE data was almost 3 times larger on 29–30 Aug as compared to the remaining days in the 26 Aug–2 Sep time period (15.9 versus $5.7 \mu g m^{-3}$, respectively). This result demonstrates how influences from typical, regional industrial sources is disrupted by the synoptic conditions that introduced the long-range transported biomass burning plumes. Although Zn and Cu have been shown to originate from wildfires

(Yamasoe et al., 2000), the averages were similar—within 1 ng m^{-3} —thus a distinct comparison could not be made within certainty. Further, these metals can also be derived from vehicular emissions, thus their concentrations may additionally be influenced by local traffic (Sternbeck et al., 2002). These results demonstrate the transport of mineral dust and biomass burning aerosol species to the Front Range, which were indeed larger in concentration during poor air quality/haze events. Interestingly, mineral dust mixed within a smoke plume from fires has predominantly been observed originating from more arid regions along the global dust belt, and using modelling or remote sensing data only (e.g., Radojevic, 2003; Tesche et al., 2009; Yang et al., 2013; Nisantzi et al., 2014). To our knowledge, this co-lofting of dust and smoke has not been shown to occur in the U.S., particularly in a region as densely covered in vegetation as the Pacific Northwest.

4 Conclusions

We have demonstrated the transport of large quantities of mineral dust and smoke/biomass burning aerosols from wildfires in the Pacific Northwest to the Colorado Front Range using a combination of in situ, remote sensing, and air parcel modelling techniques (Severignen, 2015). These aerosols were transported under synoptic conditions that contributed to three different haze events, inducing poor air quality in the Denver metro area. Three separate poor air quality events with enhanced $\text{PM}_{2.5}$ were likely dependent on the number of fires and observed to occur with cold frontal passages along Colorado's Front Range, enabling the enhanced AOD plumes originating from the Pacific Northwest wildfires to propagate south-eastward to Colorado's Front Range. Air masses were shown to originate from over the region dense with wildfires, and followed through satellite-detected aerosol plumes, which were rich in a mixture of mineral dust and smoke. Tracers for these aerosol types were also detected in situ along the Front Range, and were shown to be enhanced during periods of influence from the fires.

Overall, these unique observations were demonstrated using a complete suite of in situ and remote sensing aerosol measurements in the context of in situ meteorological observations and air mass trajectory modelling. In tandem, we utilized a real-time X-ray fluorescence spectroscopy technique using the novel and field-portable PX-375 from HORIBA, Ltd. demonstrating the utility of the instrument. Although the haze events were short lived, they demonstrate how quickly (i.e., on the order of 2 to 3 days from the fire region to the Front Range) aerosols can be transported long distances and affect air quality in regions thousands of kilometres away. Interestingly, mineral dust was observed to be co-lofted and transported within the smoke plumes, an observation not previously reported for vegetated regions such as the Pacific Northwest.

Mineral dust and smoke aerosols have disparate implications for health and climate (i.e., by serving as seeds for cloud particle formation, which impacts cloud lifetime, radiative effects, and precipitation formation mechanisms), particularly at the levels observed along the Front Range. These unique observations should be taken into account when developing health standards, seeing as not only regional urban and industrial emissions contribute to poor air quality conditions. Additionally, dust and smoke are efficient cloud forming nuclei—which impacts cloud lifetime, radiative effects, and precipitation formation mechanisms,—particularly when orographically lifted along barriers

such as the Front Range into the upper atmosphere, where cloud formation is prominent. Thus, transport of these aerosols from wildfires has broad implications for altering aerosol composition in regions far from the source.

Author contribution. J. M. C. analysed XRF data, compiled CDPHE and MODIS data, ran HYSPLIT simulations, and wrote the manuscript. P. J. N. conducted meteorological analysis and interpretation. T. C. compiled and analysed CALIPSO data. C. J. S., G. K., and R. A. analysed and supplied TOPAZ data. A. Y. provided PX-375 for usage. All co-authors contributed to the writing of or provided comments for manuscript.

Acknowledgements. The authors would like to acknowledge the many agencies and organization from which data were acquired, including the CDPHE for air quality data, NASA for MODIS and CALIPSO observations, NOAA for HYSPLIT and HMT meteorological data, and the HDF group for providing example code to process CALIPSO data.

References

- Ackerman, S. A., Strabala, K. I., Menzel, W. P., Frey, R. A., Moeller, C. C., and Gumley, L. E.: Discriminating clear sky from clouds with MODIS, *J Geophys Res-Atmos*, 103, 32141-32157, 1998.
- Alvarez, R. J., Senff, C. J., Langford, A. O., Weickmann, A. M., Law, D. C., Machol, J. L., Merritt, D. A., Marchbanks, R. D., Sandberg, S. P., Brewer, W. A., Hardesty, R. M., and Banta, R. M.: Development and Application of a Compact, Tunable, Solid-State Airborne Ozone Lidar System for Boundary Layer Profiling, *J Atmos Ocean Tech*, 28, 1258-1272, 2011.
- Alvarez, R. J., Senff, C. J., Weickmann, A. M., Sandberg, S. P., Langford, A. O., Marchbanks, R. D., Brewer, W. A., and Hardesty, R. M.: Reconfiguration of the NOAA TOPAZ lidar for ground-based measurement of ozone and aerosol backscatter, *Proceedings of the 26th International Laser Radar Conference, Porto Heli, Greece, 2012*.
- Ansmann, A., Baars, H., Tesche, M., Muller, D., Althausen, D., Engelmann, R., Pauliquevis, T., and Artaxo, P.: Dust and smoke transport from Africa to South America: Lidar profiling over Cape Verde and the Amazon rainforest, *Geophys Res Lett*, 36, 2009.
- Artaxo, P., Gerab, F., Yamasoe, M. A., and Martins, J. V.: Fine Mode Aerosol Composition at 3 Long-Term Atmospheric Monitoring Sites in the Amazon Basin, *J Geophys Res-Atmos*, 99, 22857-22868, 1994.
- Baars, H., Ansmann, A., Althausen, D., Engelmann, R., Artaxo, P., Pauliquevis, T., and Souza, R.: Further evidence for significant smoke transport from Africa to Amazonia, *Geophys Res Lett*, 38, 2011.
- Benjamin, S. G., Weygandt, S. S., Brown, J. M., Hu, M., Alexander, C., Smirnova, T. G., Olson, J. B., James, E., Dowell, D. C., Grell, G. A., Lin, H., Peckham, S. E., Smith, T. L., and Moninger, W. R.: A North American hourly assimilation and model forecast cycle: The rapid refresh, *Mon. Wea. Rev.*, 144, in review, 2016.
- Bowman, D. J. S., and Johnston, F.: Wildfire Smoke, Fire Management, and Human Health, *EcoHealth*, 2, 76-80, 2005.
- Bravo, A. H., Sosa, E. R., Sanchez, A. P., Jaimes, P. M., and Saavedra, R. M. I.: Impact of wildfires on the air quality of Mexico City, 1992-1999, *Environ Pollut*, 117, 243-253, 2002.
- Brown, S. S., Thornton, J. A., Keene, W. C., Pszenny, A. A. P., Sive, B. C., Dube, W. P., Wagner, N. L., Young, C. J., Riedel, T. P., Roberts, J. M., VandenBoer, T. C., Bahreini, R., Ozturk, F., Middlebrook, A. M., Kim, S., Hubler, G., and Wolfe, D. E.: Nitrogen, Aerosol Composition, and Halogens on a Tall Tower (NACHTT): Overview of a wintertime air chemistry field study in the front range urban corridor of Colorado, *J Geophys Res-Atmos*, 118, 8067-8085, 2013.
- Chalbot, M. C., Nikolich, G., Etyemezian, V., Dubois, D. W., King, J., Shafer, D., da Costa, G. G., Hinton, J. F., and Kavouras, I. G.: Soil humic-like organic compounds in prescribed fire emissions using nuclear magnetic resonance spectroscopy, *Environ Pollut*, 181, 167-171, 2013.
- Chang-Graham, A. L., Profeta, L. T. M., Johnson, T. J., Yokelson, R. J., Laskin, A., and Laskin, J.: Case Study of Water-Soluble Metal Containing Organic Constituents of Biomass Burning Aerosol, *Environ Sci Technol*, 45, 1257-1263, 2011.
- Clements, C. B., Zhong, S. Y., Bian, X. D., Heilman, W. E., and Byun, D. W.: First observations of turbulence generated by grass fires, *J Geophys Res-Atmos*, 113, 2008.
- Colarco, P. R., Schoeberl, M. R., Doddridge, B. G., Marufu, L. T., Torres, O., and Welton, E. J.: Transport of smoke from Canadian forest fires to the surface near Washington, D. C.: Injection height, entrainment, and optical properties, *J Geophys Res-Atmos*, 109, 2004.
- Colle, B. A., and Mass, C. F.: The Structure and Evolution of Cold Surges East of the Rocky-Mountains, *Mon Weather Rev*, 123, 2577-2610, 1995.

Cruz, C. N., and Pandis, S. N.: A study of the ability of pure secondary organic aerosol to act as cloud condensation nuclei, *Atmos Environ*, 31, 2205-2214, 1997.

Davis, C. A.: Mesoscale anticyclonic circulations in the lee of the central Rocky Mountains, *Mon Weather Rev*, 125, 2838-2855, 1997.

DeMott, P. J., Chen, Y., Kreidenweis, S. M., Rogers, D. C., and Sherman, D. E.: Ice formation by black carbon particles, *Geophys Res Lett*, 26, 2429-2432, 1999.

DeMott, P. J., Sassen, K., Poellot, M. R., Baumgardner, D., Rogers, D. C., Brooks, S. D., Prenni, A. J., and Kreidenweis, S. M.: African dust aerosols as atmospheric ice nuclei, *Geophys Res Lett*, 30, 2003.

Draxler, R. R., and Rolph, G. D.: HYSPLIT (HYbrid Single-Particle Lagrangian Integrated Trajectory) Model access via NOAA ARL READY Website (<http://ready.arl.noaa.gov/HYSPLIT.php>), 2011.

Eagan, R. C., Hobbs, P. V., and Radke, L. F.: Measurements of Cloud Condensation Nuclei and Cloud Droplet Size Distributions in Vicinity of Forest Fires, *J Appl Meteorol*, 13, 553-557, 1974.

Gadi, R., Kulshrestha, U. C., Sarkar, A. K., Garg, S. C., and Parashar, D. C.: Emissions of SO₂ and NO_x from biofuels in India, *Tellus B*, 55, 787-795, 2003.

Gaudichet, A., Echalar, F., Chatenet, B., Quisefit, J. P., Malingre, G., Cachier, H., Buatmenard, P., Artaxo, P., and Maenhaut, W.: Trace-Elements in Tropical African Savanna Biomass Burning Aerosols, *J Atmos Chem*, 22, 19-39, 1995.

Ge, C., Wang, J., and Reid, J. S.: Mesoscale modeling of smoke transport over the Southeast Asian Maritime Continent: coupling of smoke direct radiative effect below and above the low-level clouds, *Atmos Chem Phys*, 14, 159-174, 2014.

Giglio, L., Descloitres, J., Justice, C. O., and Kaufman, Y. J.: An enhanced contextual fire detection algorithm for MODIS, *Remote Sens Environ*, 87, 273-282, 2003.

Giglio, L.: MODIS Collection 5 Active Fire Product User's Guide Version 2.4, Science Systems and Applications, Inc., 2010.

Haagenson, P. L.: Meteorological and Climatological Factors Affecting Denver Air-Quality, *Atmos Environ*, 13, 79-85, 1979.

Hand, J. L., Copland, S. A., Dillner, A. M., Indresand, H., Malm, W. C., McDade, C. E., Moore, C. T., Pitchford, M. L., Schichtel, B. A., and Watson, J. G.: Spatial and Seasonal Patterns and Temporal Variability of Haze and its Constituents in the United States Report V Cooperative Institute for Research in the Atmosphere, 2011.

Hutton, M., and Symon, C.: The Quantities of Cadmium, Lead, Mercury and Arsenic Entering the Uk Environment from Human Activities, *Sci Total Environ*, 57, 129-150, 1986.

Jacob, D. J., and Winner, D. A.: Effect of climate change on air quality, *Atmos Environ*, 43, 51-63, 2009.

Jaffe, D. A., and Wigder, N. L.: Ozone production from wildfires: A critical review, *Atmos Environ*, 51, 1-10, 2012.

Jayachandran, S.: Air quality and early-life mortality: Evidence from Indonesia's wildfires, *J. Human Resources*, 44, 916-954, 2008.

Kalnay, E., Kanamitsu, M., Kistler, R., Collins, W., Deaven, D., Gandin, L., Iredell, M., Saha, S., White, G., Woollen, J., Zhu, Y., Chelliah, M., Ebisuzaki, W., Higgins, W., Janowiak, J., Mo, K. C., Ropelewski, C., Wang, J., Leetmaa, A., Reynolds, R., Jenne, R., and Joseph, D.: The NCEP/NCAR 40-year reanalysis project, *B Am Meteorol Soc*, 77, 437-471, 1996.

Kaufman, Y. J., Tanre, D., Remer, L. A., Vermote, E. F., Chu, A., and Holben, B. N.: Operational remote sensing of tropospheric aerosol over land from EOS moderate resolution imaging spectroradiometer, *J Geophys Res-Atmos*, 102, 17051-17067, 1997.

Kreidenweis, S. M., Remer, L. A., Bruantjes, R., and Dubovik, O.: Smoke aerosol from biomass burning in Mexico: Hygroscopic smoke optical model, *J Geophys Res-Atmos*, 106, 4831-4844, 2001.

Liu, Y. Q., Stanturf, J., and Goodrick, S.: Trends in global wildfire potential in a changing climate, *Forest Ecol Manag*, 259, 685-697, 2010.

Malm, W. C., Sisler, J. F., Huffman, D., Eldred, R. A., and Cahill, T. A.: Spatial and Seasonal Trends in Particle Concentration and Optical Extinction in the United-States, *J Geophys Res-Atmos*, 99, 1347-1370, 1994.

McCluskey, C. S., DeMott, P. J., Prenni, A. J., Levin, E. J. T., McMeeking, G. R., Sullivan, A. P., Hill, T. C. J., Nakao, S., Carrico, C. M., and Kreidenweis, S. M.: Characteristics of atmospheric ice nucleating particles associated with biomass burning in the US: Prescribed burns and wildfires, *J Geophys Res-Atmos*, 119, 2014.

Moore, D., Copes, R., Fisk, R., Joy, R., Chan, K., and Brauer, M.: Population Health Effects of Air Quality Changes Due to Forest Fires in British Columbia in 2003: Estimates from Physician-visit Billing Data, *Canadian Journal of Public Health / Revue Canadienne de Sante'e Publique*, 97, 105-108, 2006.

Mott, J. A., Meyer, P., Mannino, D., Redd, S. C., Smith, E. M., Gotway-Crawford, C., and Chase, E.: Wildland forest fire smoke: health effects and intervention evaluation, Hoopa, California, 1999, *Western Journal of Medicine*, 176, 157-162, 2002.

Neff, J. C., Ballantyne, A. P., Farmer, G. L., Mahowald, N. M., Conroy, J. L., Landry, C. C., Overpeck, J. T., Painter, T. H., Lawrence, C. R., and Reynolds, R. L.: Increasing eolian dust deposition in the western United States linked to human activity, *Nat Geosci*, 1, 189-195, 2008.

Neiman, P. J., Ralph, F. M., Weber, R. L., Uttal, T., Nance, L. B., and Levinson, D. H.: Observations of nonclassical frontal propagation and frontally forced gravity waves adjacent to steep topography, *Mon Weather Rev*, 129, 2633-2659, 2001.

Nisantzi, A., Mamouri, R. E., Ansmann, A., and Hadjimitsis, D.: Injection of mineral dust into the free troposphere during fire events observed with polarization lidar at Limassol, Cyprus, *Atmos Chem Phys*, 14, 12155-12165, 2014.

Nriagu, J. O.: A Global Assessment of Natural Sources of Atmospheric Trace-Metals, *Nature*, 338, 47-49, 1989.

Omar, A. H., Winker, D. M., Kittaka, C., Vaughan, M. A., Liu, Z. Y., Hu, Y. X., Trepte, C. R., Rogers, R. R., Ferrare, R. A., Lee, K. P., Kuehn, R. E., and Hostetler, C. A.: The CALIPSO Automated Aerosol Classification and Lidar Ratio Selection Algorithm, *J Atmos Ocean Tech*, 26, 1994-2014, 2009.

- Pachon, J. E., Weber, R. J., Zhang, X. L., Mulholland, J. A., and Russell, A. G.: Revising the use of potassium (K) in the source apportionment of PM_{2.5}, *Atmos Pollut Res*, 4, 14-21, 2013.
- Paciga, J. J., and Jervis, R. E.: Multielement Size Characterization of Urban Aerosols, *Environ Sci Technol*, 10, 1124-1128, 1976.
- Park, R. J., Jacob, D. J., Chin, M., and Martin, R. V.: Sources of carbonaceous aerosols over the United States and implications for natural visibility, *J Geophys Res-Atmos*, 108, 2003.
- Peterson, D., Hyer, E., and Wang, J.: Quantifying the potential for high-altitude smoke injection in the North American boreal forest using the standard MODIS fire products and subpixel-based methods, *J Geophys Res-Atmos*, 119, 3401-3419, 2014.
- Phuleria, H. C., Fine, P. M., Zhu, Y. F., and Sioutas, C.: Air quality impacts of the October 2003 Southern California wildfires, *J Geophys Res-Atmos*, 110, 2005.
- Pinker, R. T., Liu, H., Osborne, S. R., and Akoshile, C.: Radiative effects of aerosols in sub-Sahel Africa: Dust and biomass burning, *J Geophys Res-Atmos*, 115, 2010.
- Pio, C. A., Legrand, M., Alves, C. A., Oliveira, T., Afonso, J., Caseiro, A., Puxbaum, H., Sanchez-Ochoa, A., and Gelencser, A.: Chemical composition of atmospheric aerosols during the 2003 summer intense forest fire period, *Atmos Environ*, 42, 7530-7543, 2008.
- Radojevic, M.: Chemistry of forest fires and regional haze with emphasis on Southeast Asia, *Pure Appl Geophys*, 160, 157-187, 2003.
- Severignen, M.: Detecting source of unexpected peak of PM₁₀ over Flanders (Belgium): a walk through public available information, personal communication, 2015.
- Sibold, J. S., and Veblen, T. T.: Relationships of subalpine forest fires in the Colorado Front Range with interannual and multidecadal-scale climatic variation, *J Biogeogr*, 33, 833-842, 2006.
- Spracklen, D. V., Logan, J. A., Mickley, L. J., Park, R. J., Yevich, R., Westerling, A. L., and Jaffe, D. A.: Wildfires drive interannual variability of organic carbon aerosol in the western US in summer, *Geophys Res Lett*, 34, 2007.
- Sternbeck, J., Sjodin, A., and Andreasson, K.: Metal emissions from road traffic and the influence of resuspension - results from two tunnel studies, *Atmos Environ*, 36, 4735-4744, 2002.
- Streets, D. G., Yarber, K. F., Woo, J. H., and Carmichael, G. R.: Biomass burning in Asia: Annual and seasonal estimates and atmospheric emissions, *Global Biogeochem Cy*, 17, 2003.
- Tesche, M., Ansmann, A., Muller, D., Althausen, D., Engelmann, R., Freudenthaler, V., and Gross, S.: Vertically resolved separation of dust and smoke over Cape Verde using multiwavelength Raman and polarization lidars during Saharan Mineral Dust Experiment 2008, *J Geophys Res-Atmos*, 114, 2009.
- Thomaidis, N. S., Bakeas, E. B., and Siskos, P. A.: Characterization of lead, cadmium, arsenic and nickel in PM_{2.5} particles in the Athens atmosphere, Greece, *Chemosphere*, 52, 959-966, 2003.
- Toth, J. J., and Johnson, R. H.: Summer Surface Flow Characteristics over Northeast Colorado, *Mon Weather Rev*, 113, 1458-1469, 1985.
- Vali, G., DeMott, P. J., Mohler, O., and Whale, T. F.: Technical Note: A proposal for ice nucleation terminology, *Atmos Chem Phys*, 15, 10263-10270, 2015.
- VanCuren, R. A.: Asian aerosols in North America: Extracting the chemical composition and mass concentration of the Asian continental aerosol plume from long-term aerosol records in the western United States, *J Geophys Res-Atmos*, 108, 2003.
- Vaughan, M., Young, S., Winker, D., Powell, K., Omar, A., Liu, Z. Y., Hu, Y. X., and Hostetler, C.: Fully automated analysis of space-based lidar data: an overview of the CALIPSO retrieval algorithms and data products, *Bba Lib*, 5575, 16-30, 2004.
- Watson, J. G., Fujita, E., Chow, J. C., Zielinska, B., Richards, L. W., Neff, W., and Dietrich, D.: Northern Front Range Air Quality Study Final Report, 1998.
- Weber, B. L., Wuerz, D. B., and Welsh, D. C.: Quality Controls for Profiler Measurements of Winds and RASS Temperatures, *J Atmos Ocean Tech*, 10, 452-464, 1993.
- Westerling, A. L., Hidalgo, H. G., Cayan, D. R., and Swetnam, T. W.: Warming and earlier spring increase western US forest wildfire activity, *Science*, 313, 940-943, 2006.
- White, A. B., Anderson, M. L., Dettinger, M. D., Ralph, F. M., Hinojosa, A., Cayan, D. R., Hartman, R. K., Reynolds, D. W., Johnson, L. E., Schneider, T. L., Cifelli, R., Toth, Z., Gutman, S. I., King, C. W., Gehrke, F., Johnston, P. E., Walls, C., Mann, D., Gottas, D. J., and Coleman, T.: A Twenty-First-Century California Observing Network for Monitoring Extreme Weather Events, *J Atmos Ocean Tech*, 30, 1585-1603, 2013.
- Wiedinmyer, C., Quayle, B., Geron, C., Belote, A., McKenzie, D., Zhang, X. Y., O'Neill, S., and Wynne, K. K.: Estimating emissions from fires in North America for air quality modeling, *Atmos Environ*, 40, 3419-3432, 2006.
- Winker, D. M., Vaughan, M. A., Omar, A., Hu, Y. X., Powell, K. A., Liu, Z. Y., Hunt, W. H., and Young, S. A.: Overview of the CALIPSO Mission and CALIOP Data Processing Algorithms, *J Atmos Ocean Tech*, 26, 2310-2323, 2009.
- Yamasoe, M. A., Artaxo, P., Miguel, A. H., and Allen, A. G.: Chemical composition of aerosol particles from direct emissions of vegetation fires in the Amazon Basin: water-soluble species and trace elements, *Atmos Environ*, 34, 1641-1653, 2000.
- Yang, Z. F., Wang, J., Ichoku, C., Hyer, E., and Zeng, J.: Mesoscale modeling and satellite observation of transport and mixing of smoke and dust particles over northern sub-Saharan African region, *J Geophys Res-Atmos*, 118, 12139-12157, 2013.
- Zamora, R. J., Dutton, E. G., Trainer, M., McKeen, S. A., Wilczak, J. M., and Hou, Y. T.: The accuracy of solar irradiance calculations used in mesoscale numerical weather prediction, *Mon Weather Rev*, 133, 783-792, 2005.

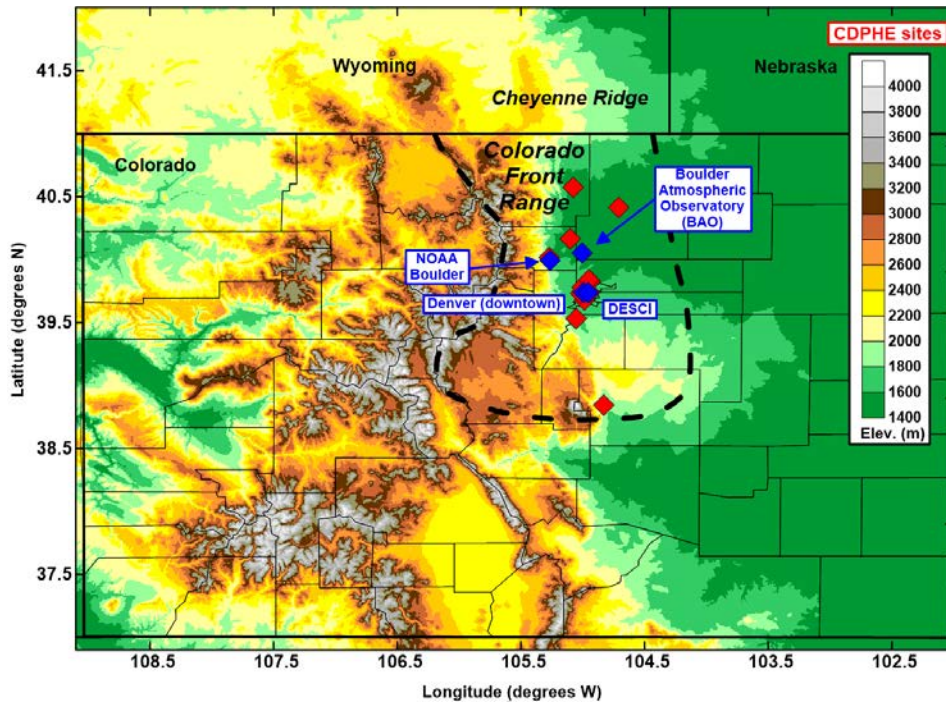


Figure 1. Map of monitoring locations, including NOAA DSRC in Boulder, which housed the PX-375 and TOPAZ lidar instruments, the BAO where the 449-MHz wind profiler was deployed, downtown Denver, the CDPHE DESC1 site where atmospheric extinction/visibility is measured, and the CDPHE sites where $PM_{2.5}$ and PM_{10} are monitored (see Table 1 for site descriptions). The approximate area encompassing the Colorado Front Range is highlighted by the dashed line. The Cheyenne Ridge in Wyoming is also notated.

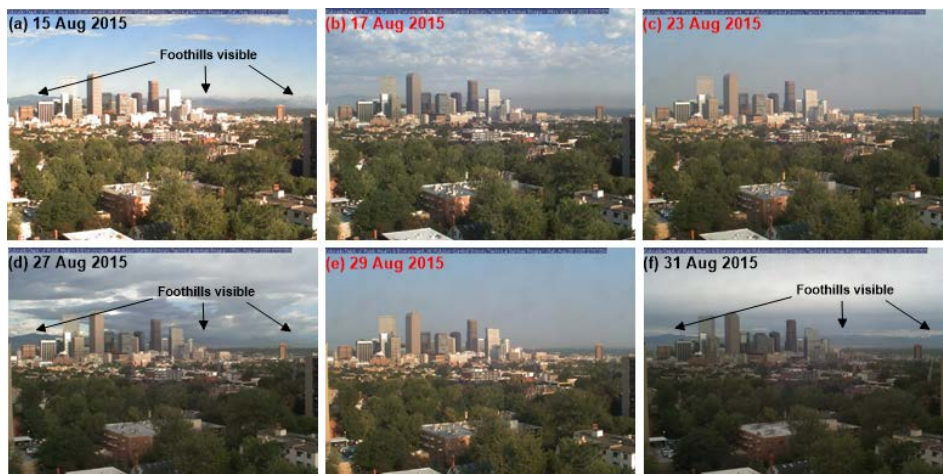


Figure 2. Images of downtown Denver facing west taken at 1400 UTC (0800 MDT). Images acquired from the CDPHE Visibility Station (DESCI; 39.73°N, 104.96°W; 1633 m MSL). Only days of significant meteorological and visibility transitions in August 2015 are shown. Days in red are those which correspond to the haziest days during the study time period. In panels (a), (d), and (f), the visibility of the foothills (and background high terrain) is highlighted.

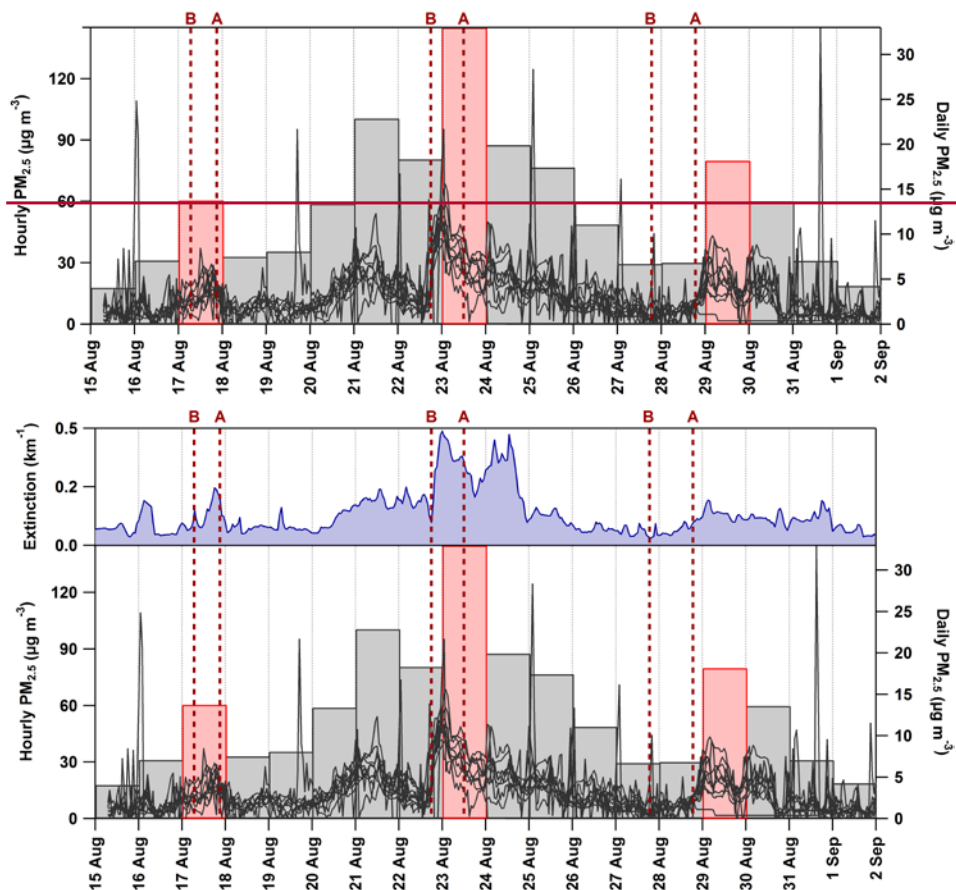


Figure 3. Top panel shows atmospheric extinction measured at the CDPHE DESC1 site (see Figure 1). Bottom panel shows hourly and daily averaged $\text{PM}_{2.5}$ mass concentrations at CDPHE sites. The pairs of red dashed lines shows the times before “B” and after “A” cold-frontal passages at BAO during or prior to each haze event. The daily averaged $\text{PM}_{2.5}$ in red represent the haziest days during or following cold front al passages (i.e., Events 1, 2, and 3 on 17, 23, and 29 Aug 2015, respectively).

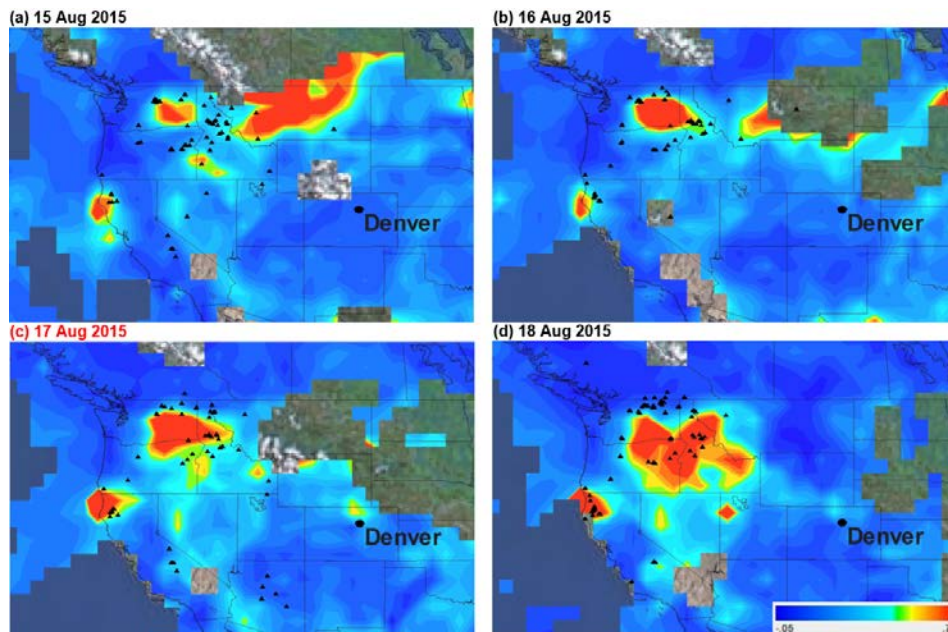


Figure 4. Daily averaged aerosol optical depth (AOD; colour bar lower right) at 550 nm and fire hotspots (black markers) detected by MODIS during the first major haze case study between 15 and 18 Aug 2015. The haziest day from the CDPHE data is labelled in red (i.e., Event 1).

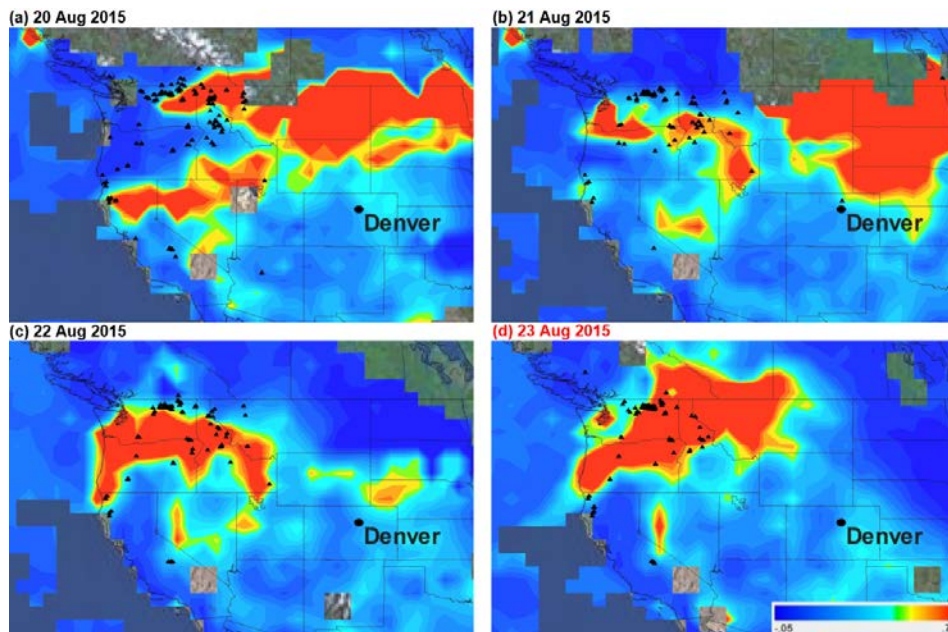


Figure 5. Same as Figure 4, but for the second major haze event between 20 and 23 Aug 2015. The haziest day from the CDPHE data is labelled in red (i.e., Event 2).

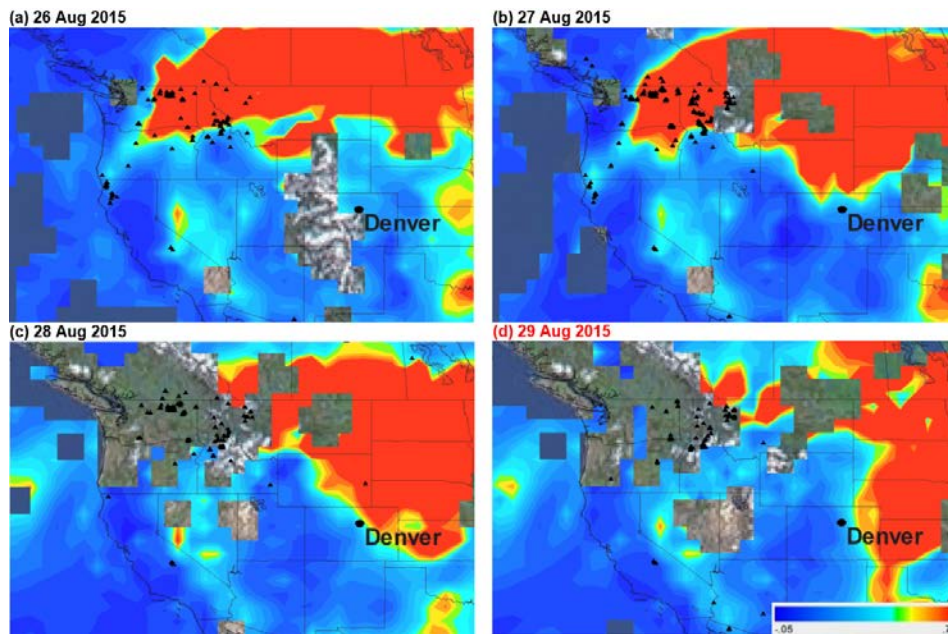


Figure 6. Same as Figure 4, but for the third major haze event between 26 and 29 Aug 2015. The haziest day from the CDPHE data is labelled in red (i.e., Event 3).

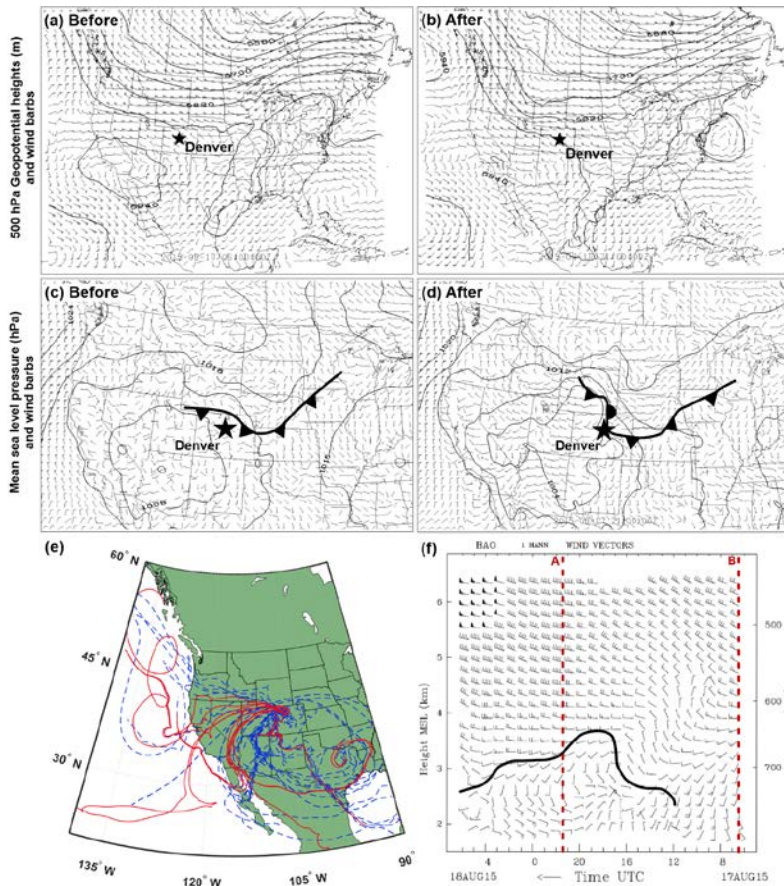


Figure 7. Meteorological analysis for Event 1 (17 Aug 2015). Top row shows 13-km resolution RAP gridded dataset of 500-hPa geopotential heights (black contours) with 500-hPa wind velocities (flags = 25 m s^{-1} , barbs = 5 m s^{-1} , half-barbs = 2.5 m s^{-1}) from Plan-view analyses from before (a) and after (b) the passage of a cold front during Event 1 at: 0600 and 2100 UTC 17 Aug 2015, respectively. Middle row shows mean sea-level pressure (black contours) with near-surface wind velocities (flags and barbs as above) from before (c) and after (d) the cold-front passage. Analyses include the 13-km-resolution RAP-gridded dataset of (left column) 500-hPa geopotential heights (m, black contours) with 500-hPa wind velocities (flags = 25 m s^{-1} , barbs = 5 m s^{-1} , half-barbs = 2.5 m s^{-1}) and (right column) mean sea-level pressure (mb, black contours) with near-surface wind velocities (flags and barbs as above). Standard frontal notation is used. (e) 10-day air mass backward trajectories initiated every 6 hours at 500, 1000, and 2000 m MSL during the time period surrounding Event 1 (15–18 Aug). Trajectories in red correspond to the haziest day (17 Aug) and the blue dashed trajectories show the remaining. (f) Time-height section of hourly-averaged wind profiles from the 449-MHz wind profiler at

639 BAO between 0600 UTC 17 Aug and 0600 UTC 18 Aug (flags and barbs are as above). The bold black line
640 denotes the approximate frontal shear boundary. The pair of red dashed lines shows the RAP analysis times
641 before “B” and after “A” the cold-frontal passage at BAO. Time increases from right to left to portray the
642 advection of upper-level synoptic features from west to east.

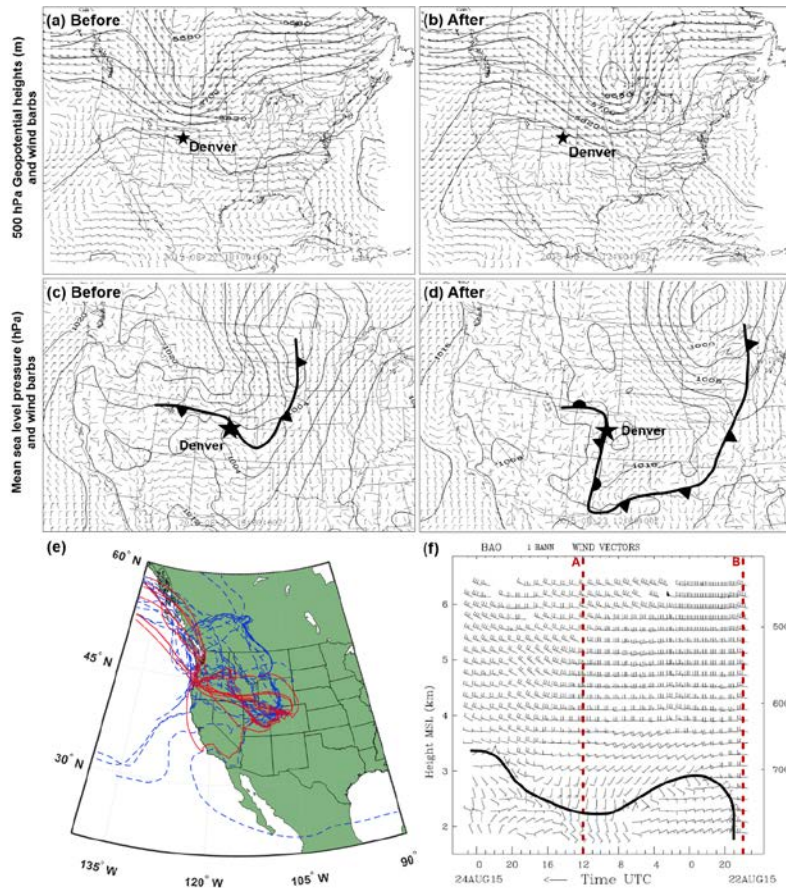


Figure 8. Air-mass backward-trajectories for all three cases where haze infiltrated the Front Range. Trajectories shown were initiated every 6 hours during time periods (i.e., cases) surrounding each event (15–18 Aug 2015, 20–23 Aug 2015, and 26–29 Aug 2015 for Cases 1, 2, and 3, respectively), include those starting at 500, 1000, and 2000 m MSL, and extend back 10 days. Trajectories in red correspond to the haziest days (i.e., Events 1, 2, and 3 on 17, 23, and 29 Aug 2015, respectively) during each case time period and the blue-dashed trajectories show the remaining days that correspond to those in the MODIS figures for each case. Same as Figure 7, but for Event 2 (23 Aug 2015). Before and after the cold-frontal passage correspond to 1800 UTC 22 Aug and 1200 UTC 23 Aug, respectively. Trajectories were initiated for the time period surrounding Event 2 (20–23 Aug). Time-height section measurements were between 1700 UTC 22 Aug and 0100 UTC 24 Aug.

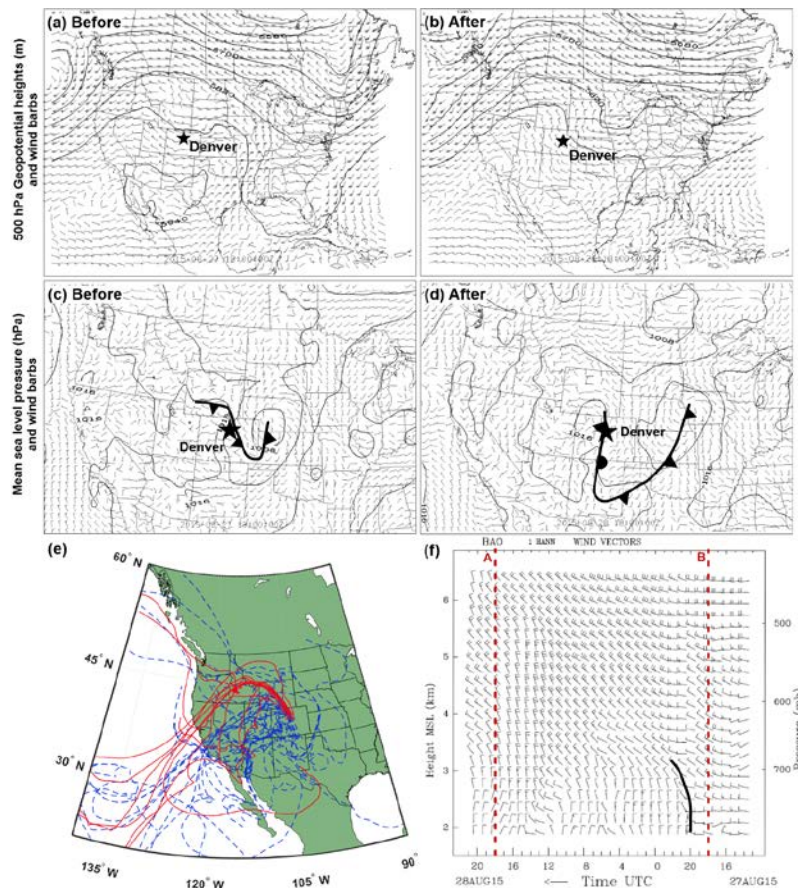


Figure 9. Same as Figure 7, but for Event 3 (29 Aug 2015). Before and after the cold-frontal passage correspond to 1800 UTC 27 Aug and 1800 UTC 28 Aug, respectively. Trajectories were initiated for the time period surrounding Event 3 (26–29 Aug). Time-height section measurements were between 1300 UTC 27 Aug and 2100 UTC 28 Aug. Time-height section of hourly-averaged wind profiles for Event 1 from the 449-MHz wind profiler at BAO between 0600 UTC 17 Aug and 0600 UTC 18 Aug 2015 (flags and barbs are as in Figure 7). The bold black line denotes the approximate frontal shear boundary. The pair of red dashed lines shows the RAP analysis times before “B” and after “A” the cold-frontal passage at BAO during Event 1. Time increases from right to left to portray the advection of upper-level synoptic features from west to east.

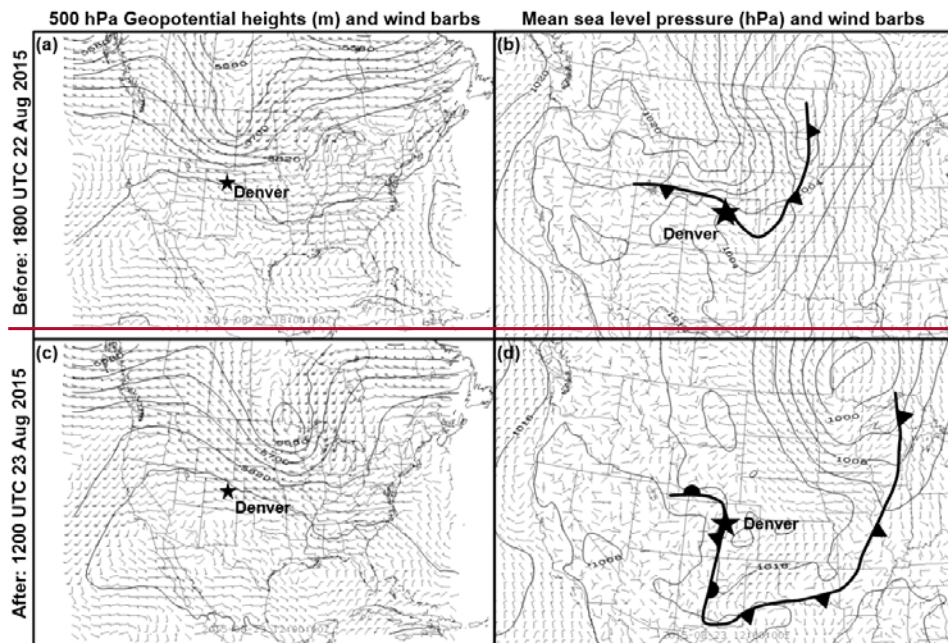


Figure 10. Same as Figure 7, but for before and after the cold-frontal passage of Event 2: 1800 UTC 22 Aug and 1200 UTC 23 Aug 2015, respectively.

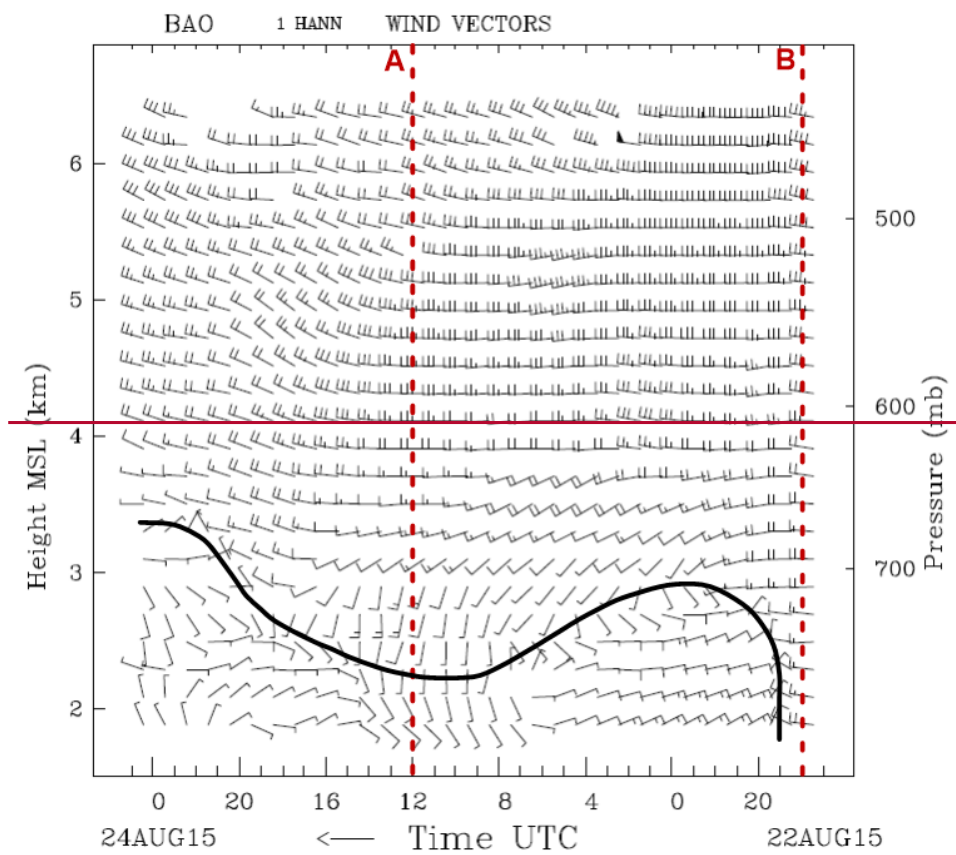


Figure 11. As in Figure 9, but for the time period between 1700 UTC 22 Aug and 0100 UTC 24 Aug during Event 2.

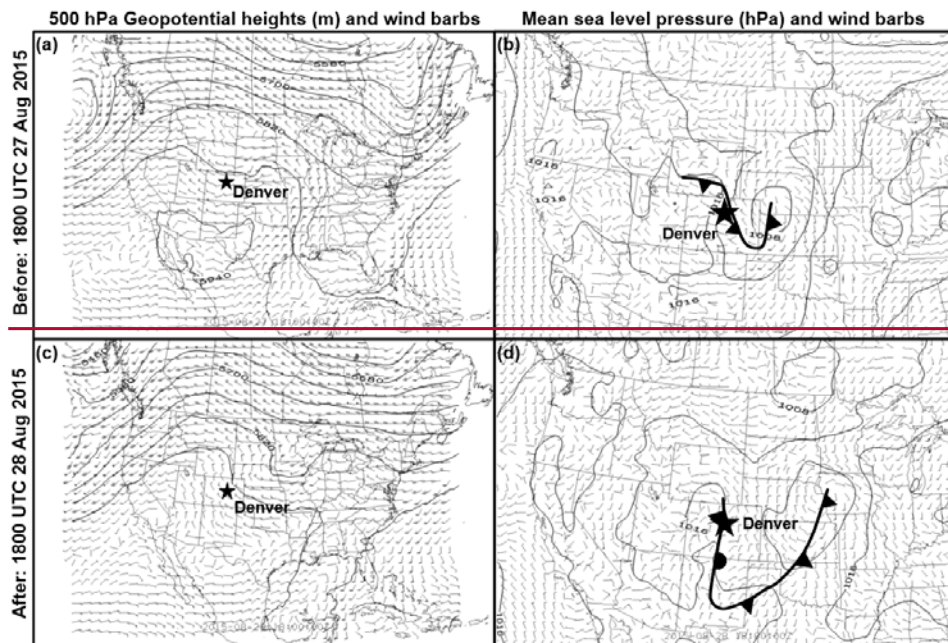


Figure 12. As in Figure 7, but for before and after the cold-frontal passage of Event 3: 1800 UTC 27 Aug and 1800 UTC 28 Aug 2015, respectively.

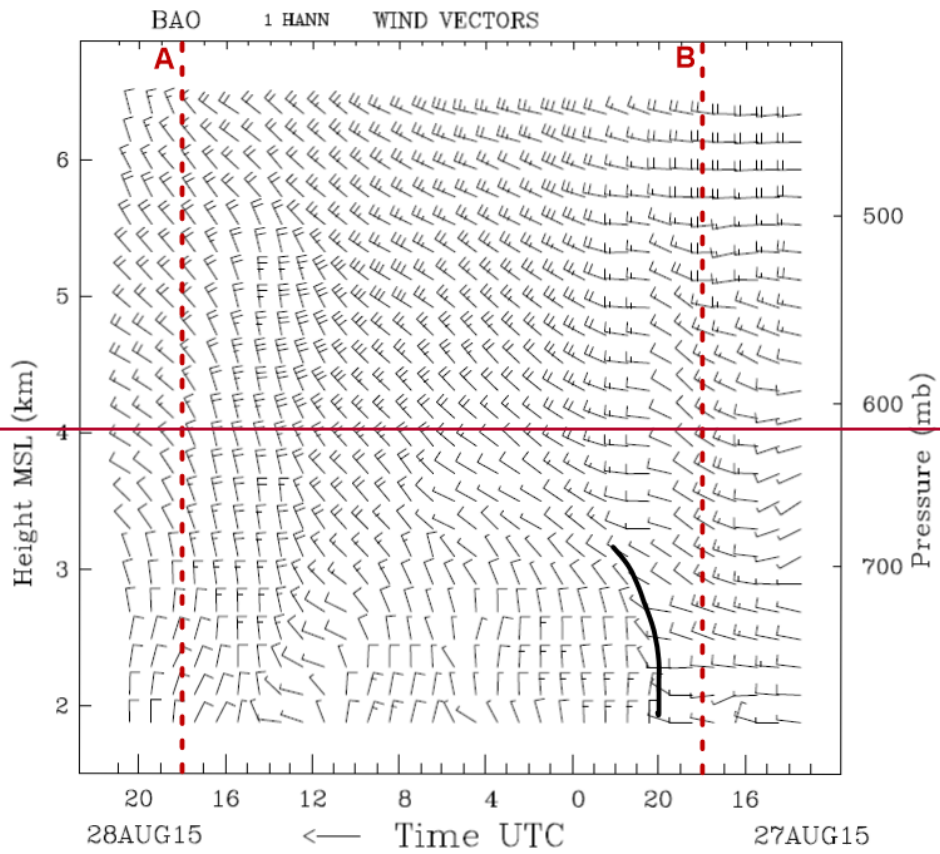


Figure 13. As in Figure 9, but for the time period between 1300 UTC 27 Aug and 2100 UTC 28 Aug during Event 3.

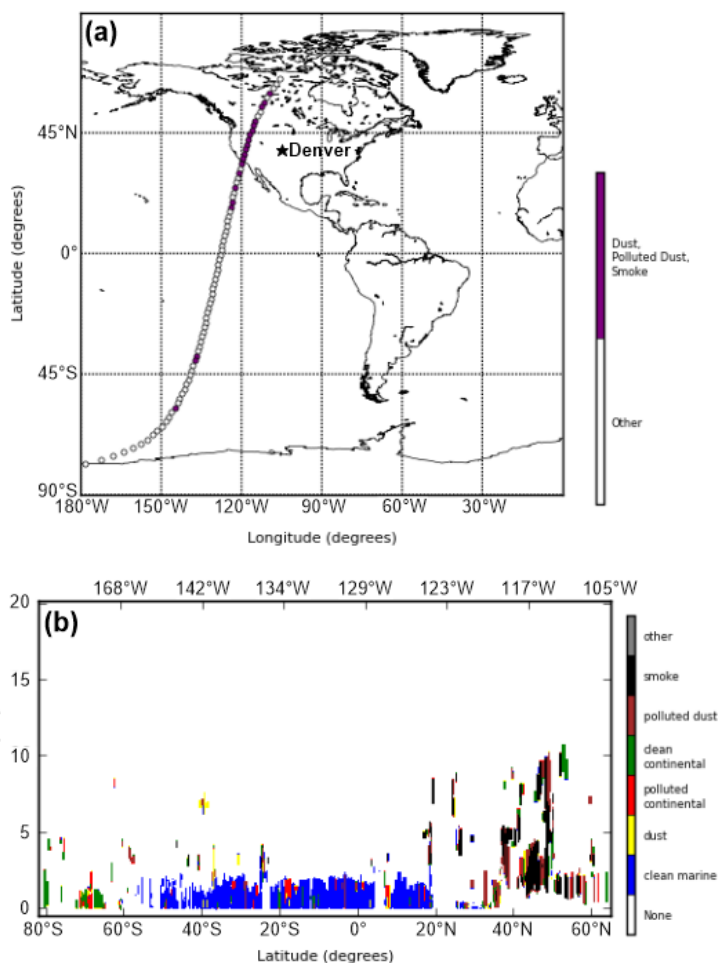


Figure 10. CALIPSO swath data from the night prior to Event 1. Swath data contained in CAL_LID_L2_VFM_ValState1-V3-30 file [are](#) from 16 Aug 2015 09:57:00 UTC. (a) Map showing CALIPSO coverage, with the purple markers representing locations in the column measurement where dust, smoke, or polluted dust were observed. (b) Vertical profile (in km MSL) for all aerosol subtypes of the swath corresponding to (a).

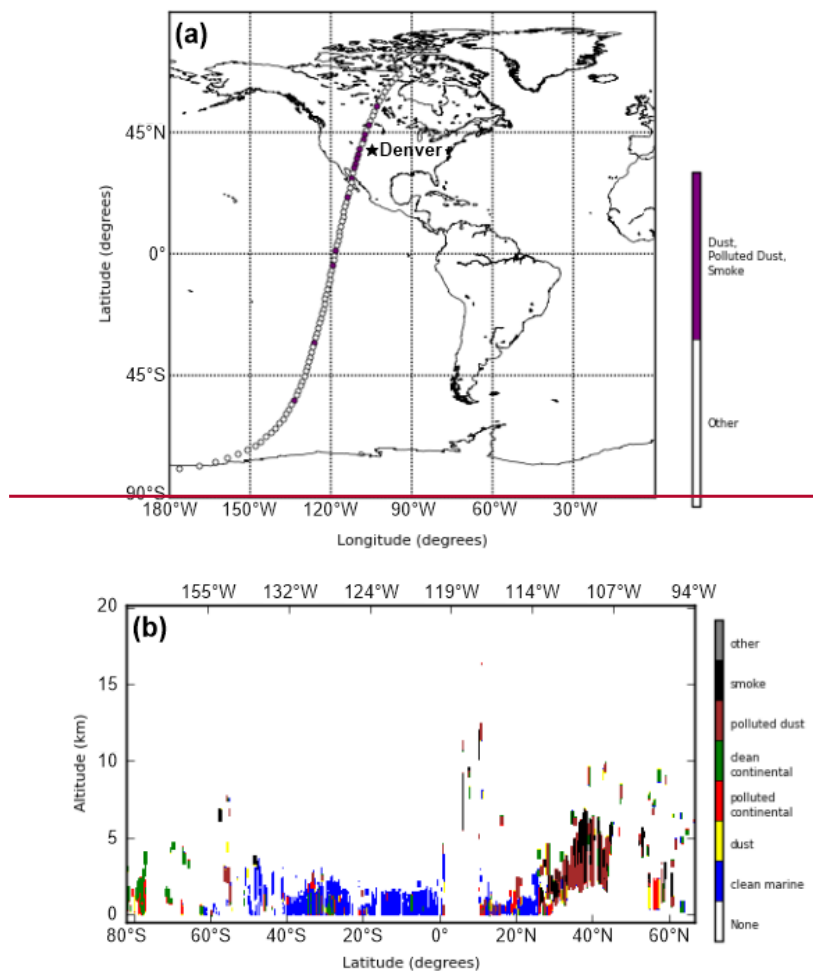


Figure 15. Same as Figure 14, but for the night prior to Event 2 and from 22 Aug 2015 09:19:24 UTC.

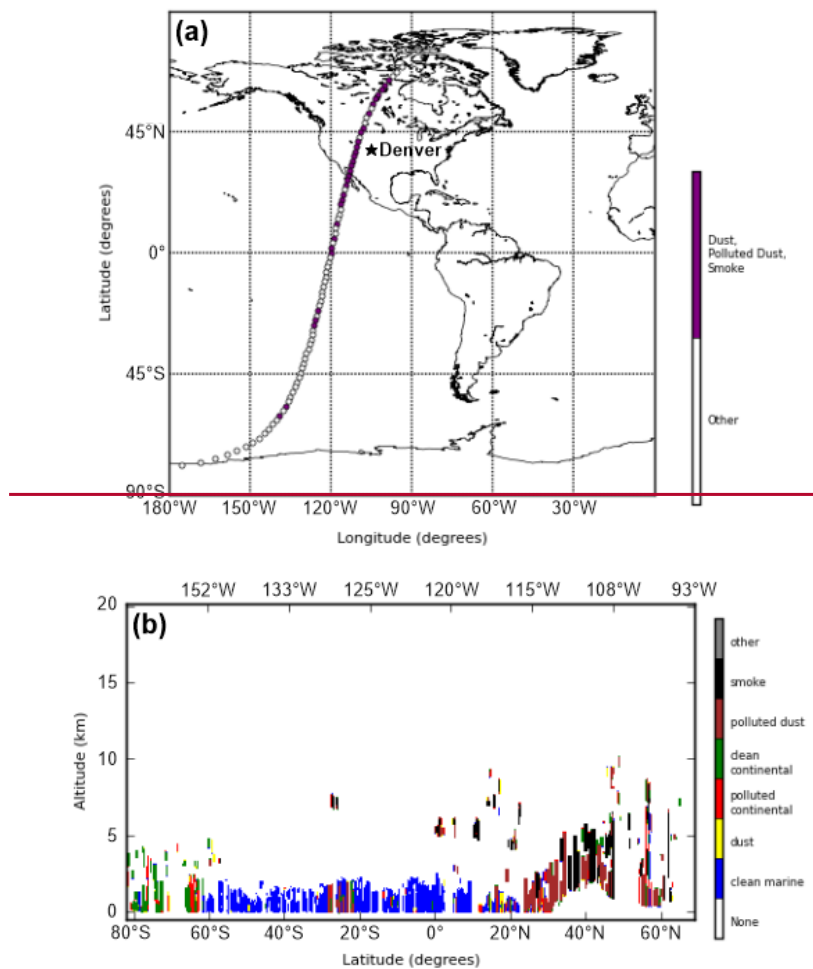


Figure 16. Same as Figure 14, but for the day of Event 3 and from 29 Aug 2015 09:24:15 UTC.

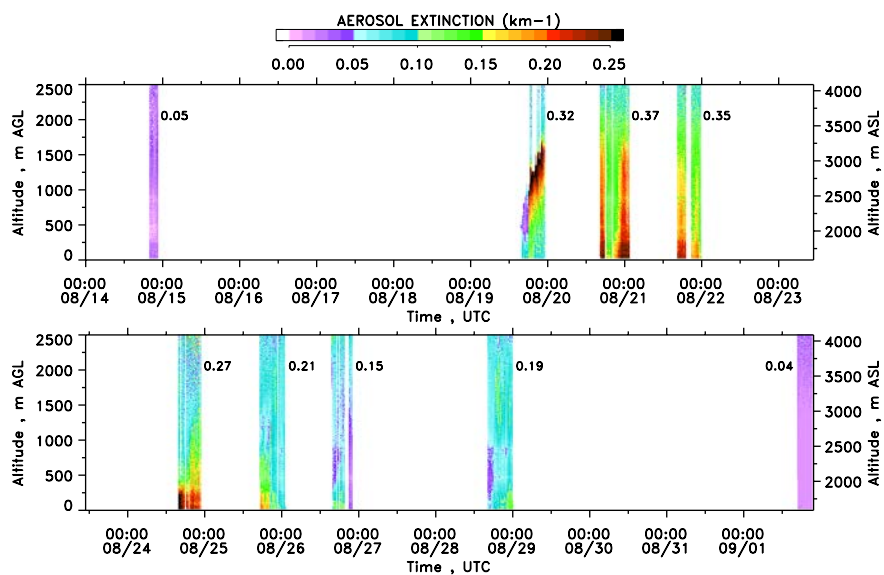
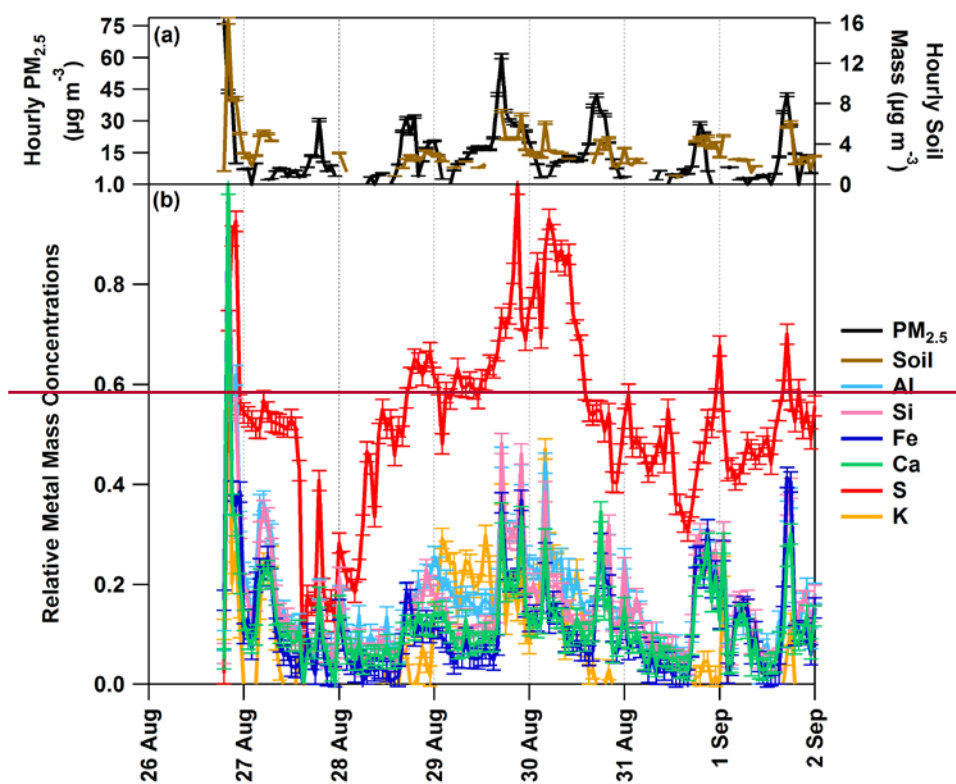


Figure 11. Aerosol extinction profiles at 294 nm observed with the TOPAZ lidar on 9 days during the smoke pollution episodes. The numbers next to each day's observations represent the daily mean AOD from the surface up to 2.5 km AGL computed from the lidar measurements.



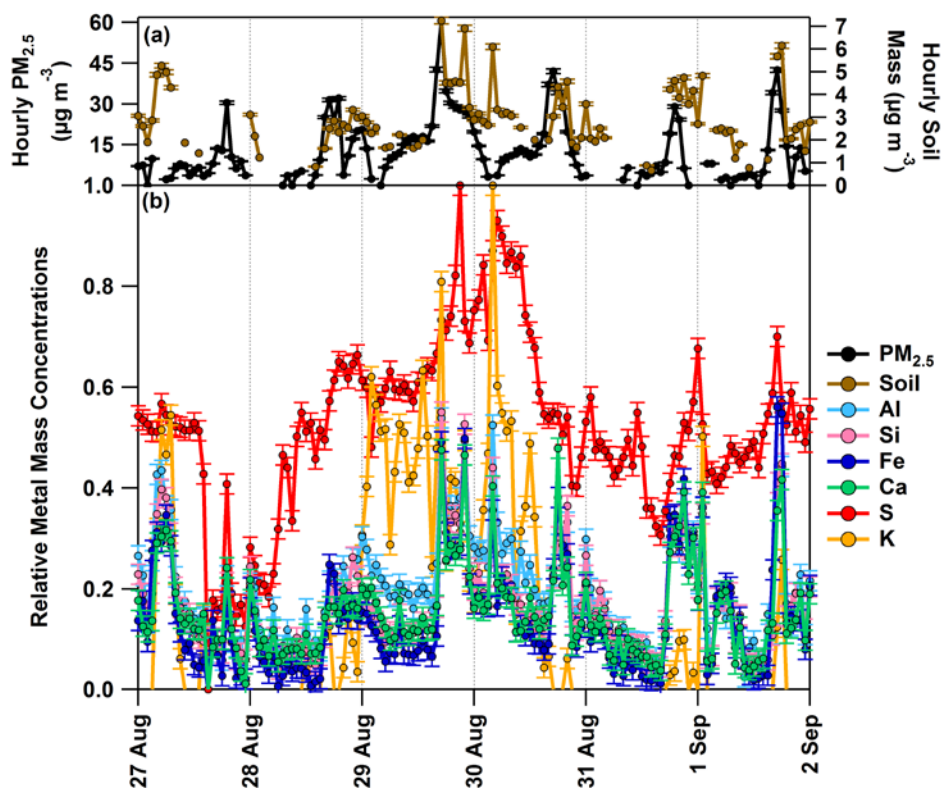


Figure 12. (a) Time series of hourly $PM_{2.5}$ and soil mass concentrations as measured by PX-375 between 27 Aug and 2 Sep 2015 and (b) relative hourly mass concentrations of select individual metals relative to their maximum concentration observed during the study time period over the LDLs, including an error of $\pm 2\%$. Only data higher than the LDLs are shown. PX-375 data overlapped with Event 3.

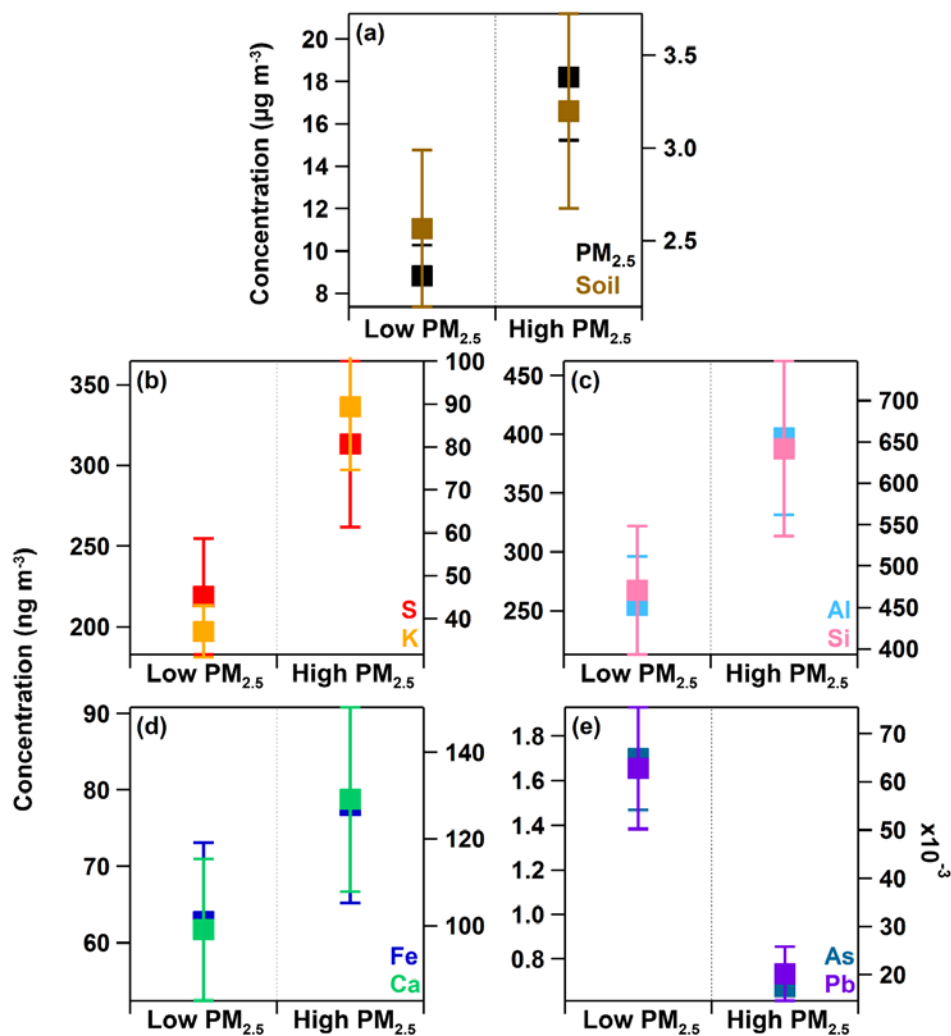


Figure 13. Averages of (a) $PM_{2.5}$ and soil concentrations, and (b) – (e) select metal mass concentrations during non-event days (i.e., cleaner conditions) compared to averages from haze event days (i.e., influence from fires haze) for 26 Aug–2 Sep 2015. “Low” and “high” correspond to the $PM_{2.5}$ concentration values. Error bars represent the 90% confidence intervals. Concentration averages were statistically significant based on t-tests of two samples of unequal variances.

Table 1. CDPHE sites used for particulate data within the Colorado Front Range. Each site has an ‘x’ for each measurement it maintained throughout the current work. Elevation is provided in meters above mean sea level (m MSL).

City/Site Name	Site ID	Latitude (degrees N)	Longitude (degrees W)	Elevation (m MSL)	PM _{2.5}	PM ₁₀
Boulder - CU/Athens	BOU	40.01	105.27	1,621	x	
Chatfield Park	CHAT	39.53	105.05	1,685	x	
Colorado College	CCOL	38.85	104.83	1,833	x	
Commerce City/Alsup Elementary	COMM	39.83	104.94	1,565	x	
Denver - Continuous Air Monitoring site	CAMP	39.68	104.99	1,610	x	x
Denver - National Jewish Health	NJH	39.74	104.94	1,615	x	
Fort Collins - CSU Facilities	FTCF	40.57	105.08	1,525	x	x
Greeley - Hospital	GREH	40.42	104.71	1,439	x	
I-25 - Denver	I-25	39.73	105.02	1,586	x	x
La Casa	CASA	39.78	105.01	1,601	x	x
Longmont - Municipal	LNGM	40.16	105.10	1,517	x	
Welby	WBY	39.84	104.95	1,554		x

PM_{2.5} = particulate matter with diameters ≤ 2.5 µm

5 PM₁₀ = particulate matter with diameters ≤ 10 µm

Table 2. Lower detection limits (LDLs, ng m⁻³) for metals measured by the PX-375 during 15 Aug–2 Sep 2015. **Data Concentrations** less than the LDLs were excluded from analysis.

Species	LDL
Ti	2.29
V	0.23
Cr	0.61
Mn	0.93
Fe	1.51
Ni	0.33
Cu	0.78
Zn	1.21
As	0.02
Pb	0.80
Al	32.2
Si	5.17
S	1.11
K	4.37
Ca	1.18

Supporting Information

Colorado air quality impacted by long-range transported aerosol: A set of case studies during the 2015 Pacific Northwest fires

Jessie M. Creamean^{1,2*}, Paul. J. Neiman², Timothy Coleman^{1,2}, Christoph J. Senff^{1,3}, Guillaume Kirgis^{1,3}, Raul J. Alvarez³, and Atsushi Yamamoto⁴

¹University of Colorado at Boulder, Cooperative Institute for Research in Environmental Sciences, Boulder, CO, 80309, USA

²NOAA Earth System Research Laboratory, Physical Sciences Division, Boulder, CO, 80305, USA

³NOAA Earth System Research Laboratory, Chemical Sciences Division, Boulder, CO, 80305, USA

⁴HORIBA Instruments Inc., Process and Environmental, Irvine, CA, 92618, USA

Correspondence to: Jessie M. Creamean (jessie.creamean@noaa.gov)

Abstract. Biomass burning plumes containing aerosols from forest fires can be transported long distances, which can ultimately impact climate and air quality in regions far from the source. Interestingly, these fires can inject aerosols other than smoke into the atmosphere, which very few studies have evidenced. Here, we demonstrate a set of case studies of long-range transport of mineral dust aerosols in addition to smoke from numerous forest fires in the Pacific Northwest to Colorado, U.S. These aerosols were detected in Boulder, Colorado along the Front Range using Beta-ray attenuation and energy dispersive X-ray fluorescence spectroscopy, and corroborated with satellite-borne lidar observations of smoke and dust. Further, we examined the transport pathways of these aerosols using air mass trajectory analysis and regional and synoptic scale meteorological dynamics. Three separate events with poor air quality and increased mass concentrations of metals from biomass burning (S and K) and minerals (Al, Si, Ca, Fe, and Ti) occurred due to the introduction of smoke and dust from regional and synoptic scale winds. Cleaner time periods with good air quality and lesser concentrations of biomass burning and mineral metals between the haze events were due to the advection of smoke and dust away from the region. Dust and smoke present in biomass burning haze can have diverse impacts on visibility, health, cloud formation, and surface radiation. Thus, it is important to understand how aerosol populations can be influenced by long-range transported aerosols, particularly those emitted from large source contributors such as forest fires.

Keywords. Aerosol transport, air quality, mineral dust, biomass burning, remote sensing, in situ observations

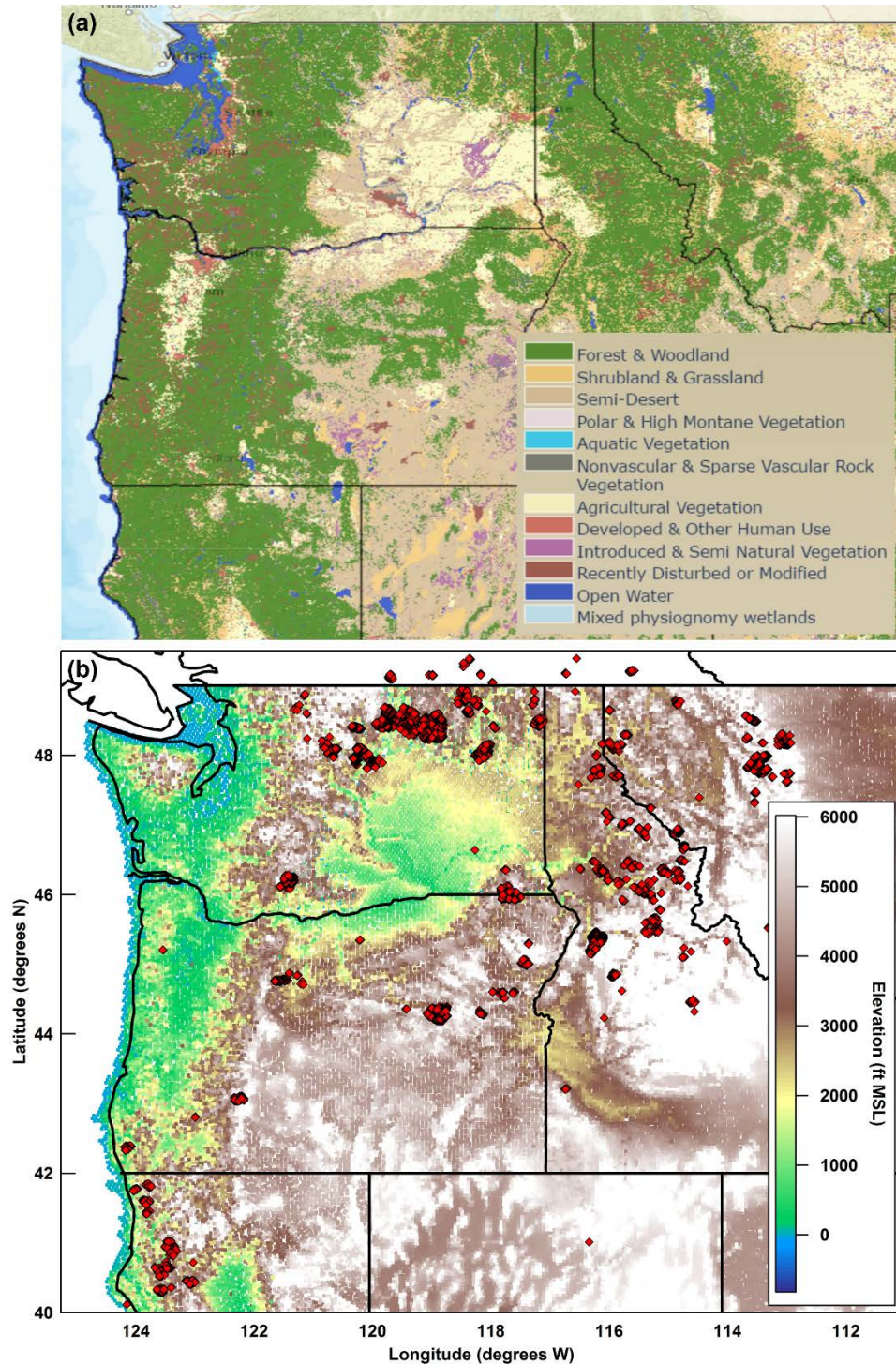


Figure S1. (a) Land cover data from the U.S. Geological Survey determined using multi-season satellite imagery from 1999–2001 in conjunction with digital elevation model (DEM) derived datasets (e.g. elevation, landform) to model natural and semi-natural vegetation (http://gis1.usgs.gov/csas/gap/viewer/land_cover/Map.aspx). (b) Elevation data from the U.S. Forest Service (http://apps.fs.fed.us/fiadb-downloads/CSV/datamart_csv.html; surveys vary by state, but were conducted 1989–2014) in addition to all MODIS thermal anomalies (i.e., fire hotspots) detected during the study time period. Fires occurred on higher elevation forest, shrub, and grass lands, but predominantly in forested or woodland areas. Few fires occurred on lower elevation agricultural lands.

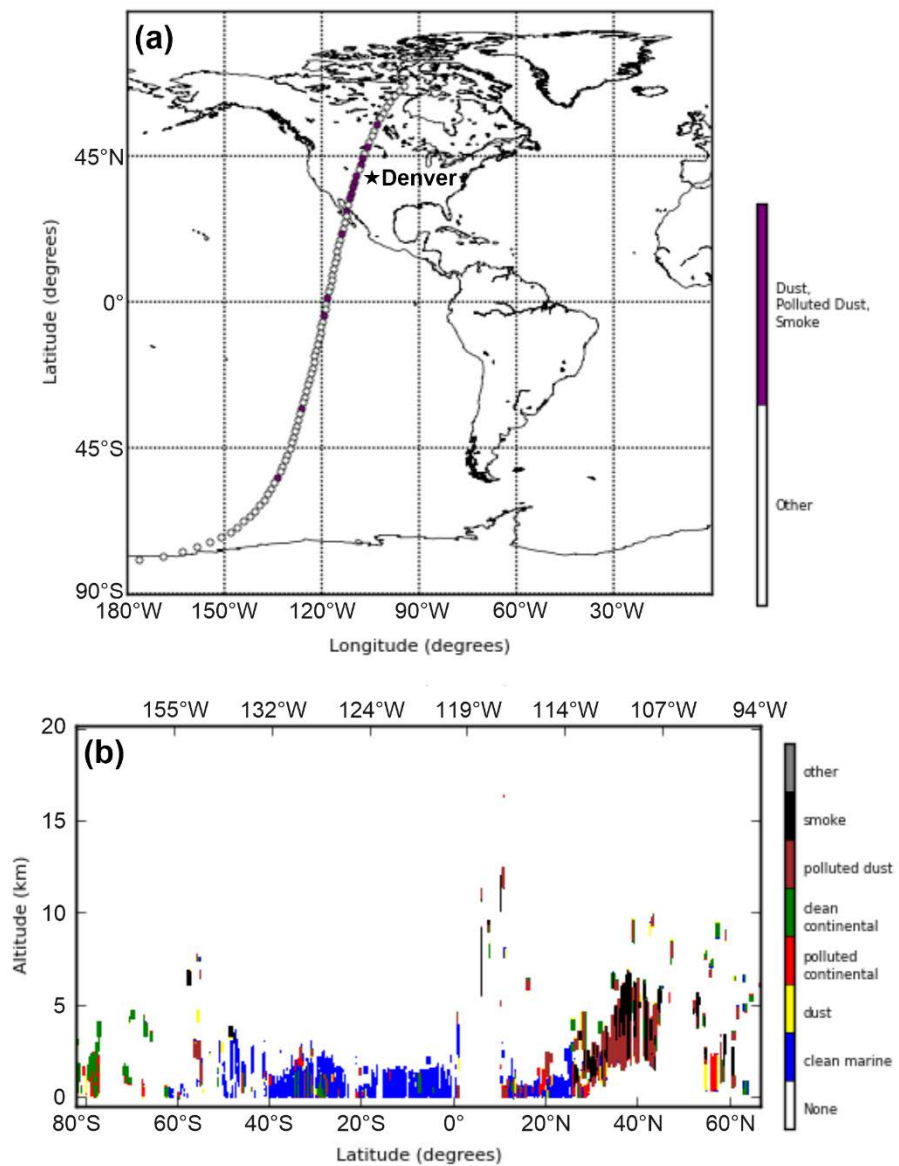


Figure S2. Same as Figure 10 in the manuscript, but for the night prior to Event 2 and from 22 Aug 2015 09:19:24 UTC.

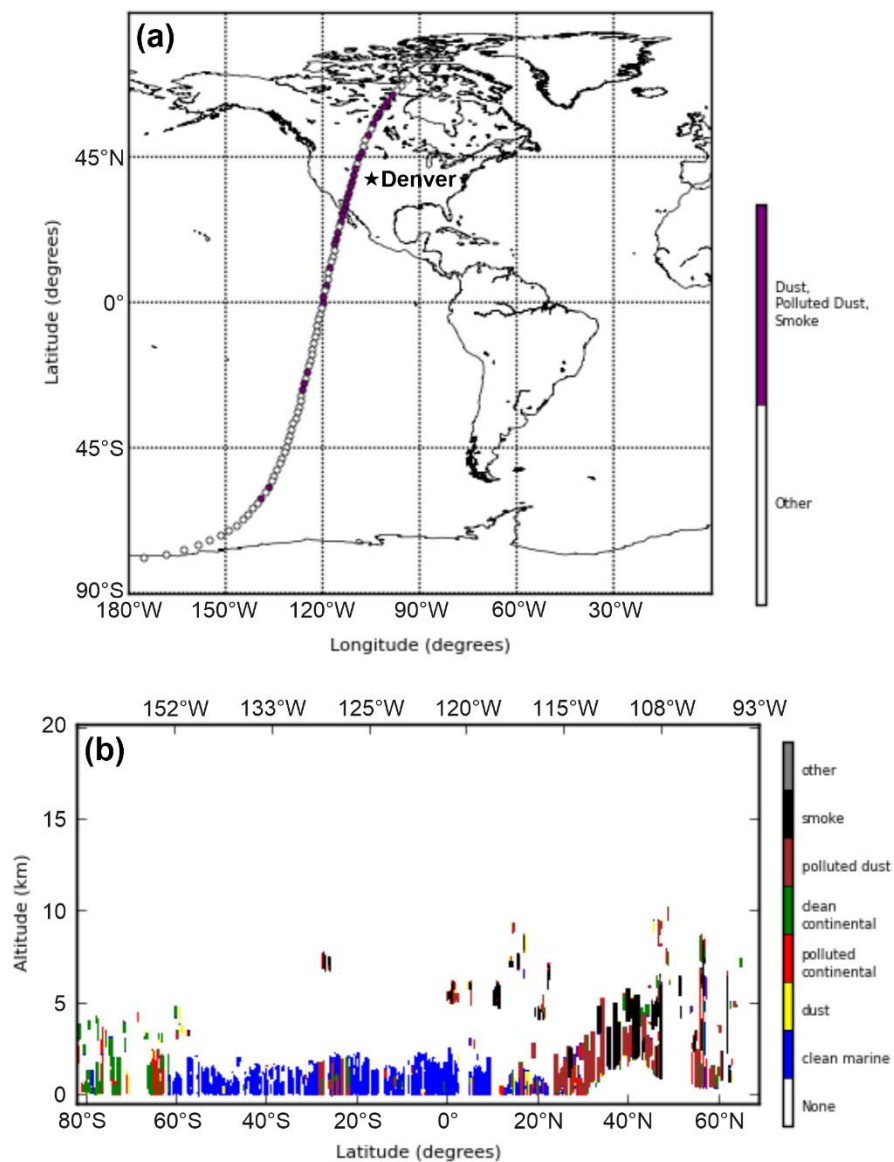


Figure S3. Same as Figure 10 in the manuscript, but for the day of Event 3 and from 29 Aug 2015 09:24:15 UTC.

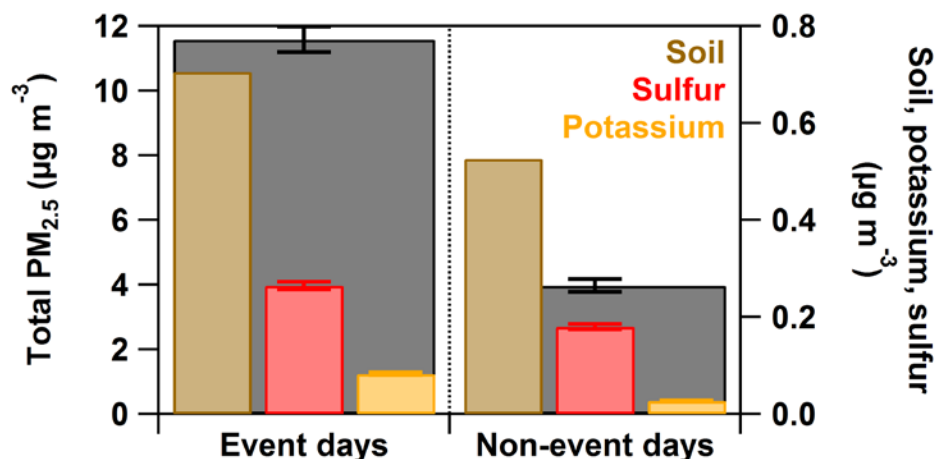


Figure S4. Concentrations of total PM_{2.5}, soil, S, and K from the IMPROVE monitoring site in Rocky Mountain National Park (ROMO; 40.28°N, 105.55°W; 2,760 m MSL) during event days and non-event days during the month of August 2015. Data and information on sampling and analytical protocols are found at <http://views.cira.colostate.edu/fed/> (Malm et al., 1994; Hand et al., 2011). Eleven samples were collected and analyzed during this time period. Uncertainty values are provided by IMPROVE for total mass and element concentration measurements (S and K), but not soil.

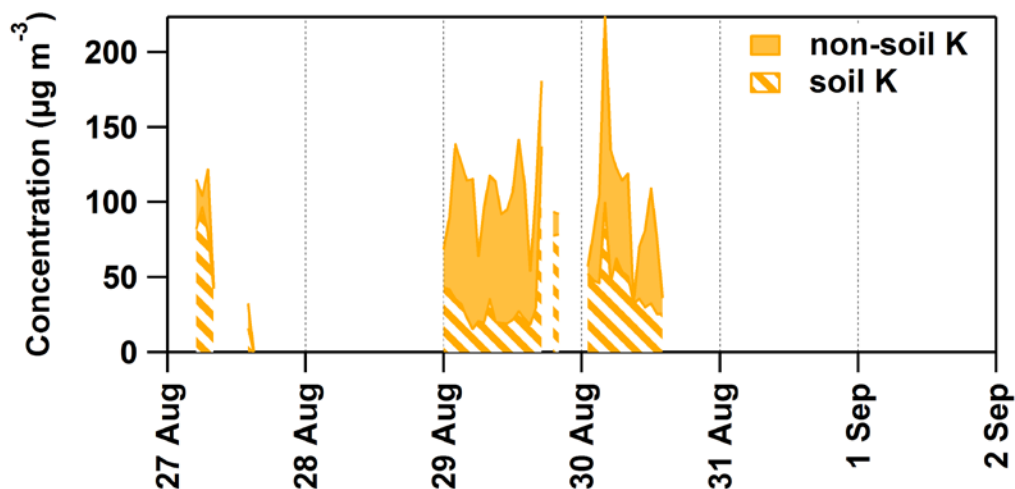


Figure S5. Non-soil and soil K concentrations measured by the PX-375 during the study time period. Concentrations were calculated from total K based on the methods on Kreidenweis et al. (2001), where [non-soil K] = [K] – 0.6[Fe] and [soil K] = [total K] – [non-soil K]. It is apparent that non-soil K and soil K were present during the Event 3 time period when the PX-375 was operable. Time periods without measurements were due to the K concentrations being below the LDL.

References

- Hand, J. L., Copland, S. A., Dillner, A. M., Indresand, H., Malm, W. C., McDade, C. E., Moore, C. T., Pitchford, M. L., Schichtel, B. A., and Watson, J. G.: Spatial and Seasonal Patterns and Temporal Variability of Haze and its Constituents in the United States Report V Cooperative Institute for Research in the Atmosphere, 2011.
- Kreidenweis, S. M., Remer, L. A., Bruintjes, R., and Dubovik, O.: Smoke aerosol from biomass burning in Mexico: Hygroscopic smoke optical model, *J Geophys Res-Atmos*, 106, 4831-4844, 2001.

Malm, W. C., Sisler, J. F., Huffman, D., Eldred, R. A., and Cahill, T. A.: Spatial and Seasonal Trends in Particle Concentration and Optical Extinction in the United-States, *J Geophys Res-Atmos*, 99, 1347-1370, 1994.